EMBRY-RIDDLE
Aeronautical University™
SCHOLARLY COMMONS

Publications

Metal Abundances and Kinematics of Bright Metal-Poor Giants Selected from the Lse Survey: Implications for the Metal-Weak Thick Disk

Timothy C. Beers
Cerro Tololo Inter-American Observatory, National Optical Astronomy Observatory, European Southern Oabservatory, beers@pa.msu.edu

John S. Drilling
Cerro Tololo Inter-American Observatory, National Optical Astornomy Observatory, drilling@rouge.phys.lse.edu

Silvia Rossi
Cerro Tololo Inter-American Observatory, National Optical Astronomy Observatory, European Southern Oabservatory, rossi@astro.iag.usp.br

Masashi Chiba
National Astronomical Observatory, Mitaka Tokyo, Japan, chibams@gala.mtk.nao.ac.jp

Jaehyon Rhee
University of Virginia, rhee@virginia.edu

Follow this and additional works at: https://commons.erau.edu/publication

Part of the Stars Interstellar Medium and the Galaxy Commons
See next page for additional authors

Scholarly Commons Citation

Authors

Timothy C. Beers, John S. Drilling, Silvia Rossi, Masashi Chiba, Jaehyon Rhee, Birgit Fŭhrmeister, John E. Norris, and Ted von Hippel

METAL ABUNDANCES AND KINEMATICS OF BRIGHT METAL-POOR GIANTS SELECTED FROM THE LSE SURVEY: IMPLICATIONS FOR THE METAL-WEAK THICK DISK

TIMOTHY C. BEERS[1,2]

Department of Physics and Astronomy, Michigan State University, East Lansing, MI 48824; beers@pa.msu.edu

JOHN S. DRILLING[1]

Department of Physics and Astronomy, Louisiana State University, Baton Rouge, LA 70803; drilling@rouge.phys.lse.edu

SILVIA ROSSI[1,2]

Instituto Astronômico e Geofísico, Universidade de São Paulo, Av. Miguel Stefano 4200, 04301-908 São Paulo, Brazil; rossi@astro.iag.usp.br

MASASHI CHIBA

National Astronomical Observatory, Mitaka, Tokyo 181-8588, Japan; chibams@gala.mtk.nao.ac.jp

JAEHYON RHEE

Department of Astronomy, University of Virginia, P.O. Box 3818, Charlottesville, VA 22903; rhee@virginia.edu

BIRGIT FÜHRMEISTER[2]

Hamburger Sternwarte, Universität Hamburg, Gojensbergsweg 112, D-21029 Hamburg, Germany; bfuhrmeister@hs.uni-hamburg.de

JOHN E. NORRIS

Mount Stromlo Observatory, Research School of Astronomy and Astrophysics, Australian National University, Cotter Road, Weston, ACT 2611, Australia; jen@mso.anu.edu.au

AND

TED VON HIPPEL

Department of Astronomy, University of Texas at Austin, Austin, TX 78712; ted@astro.as.utexas.edu

ABSTRACT

We report medium-resolution (1–2 Å) spectroscopy and broadband (*UBV*) photometry for a sample of 39 bright stars (the majority of which are likely to be giants) selected as metal-deficient candidates from an objective-prism survey concentrating on Galactic latitudes below $|b| = 30°$, the Luminous Stars Extension (LSE) survey of Drilling & Bergeron. Although the primary purpose of the LSE survey was to select OB stars (hence the concentration on low latitudes), the small number of bright metal-deficient giant candidates noted during this survey provide interesting information on the metal-weak thick disk (MWTD) population. Metal abundance estimates are obtained from several different techniques and calibrations, including some that make use of the available photometry and spectroscopy and others that use only the spectroscopy; these methods produce abundance estimates that are consistent with one another and should be secure. All of the targets in our study have available high-quality proper motions from the *Hipparcos* or Tycho II catalogs, or both, that we combine with radial velocities from our spectroscopy to obtain full space motions for the entire sample. The rotational (V_ϕ) velocities of the LSE giants indicate the presence of a rapidly rotating population, even at quite low metallicity. We consider the distribution of orbital eccentricity of the LSE giants as a function of [Fe/H] and conclude that the local fraction (i.e., within 1 kpc from the Sun) of metal-poor stars that might be associated with the MWTD is on the order of 30%–40% at abundances below [Fe/H] = −1.0. Contrary to recent analyses of previous (much larger) samples of nonkinematically selected metal-poor stars (assembled primarily from prism surveys that concentrated on latitudes above $|b| = 30°$), we find that this relatively high fraction of local metal-poor stars associated with the MWTD may extend to metallicities *below* [Fe/H] = −1.6, much lower than had been considered before. We identify a subsample of 11 LSE stars that are very likely to be members of the MWTD, based on their derived kinematics; the lowest metallicity among these stars is [Fe/H] = −2.35. Implications of these results for the origin of the MWTD and for the formation of the Galaxy are considered.

Key words: Galaxy: abundances — Galaxy: halo — Galaxy: kinematics and dynamics — stars: Population II — surveys

1. INTRODUCTION

Although considerable efforts have been made over the past few decades to identify metal-deficient stars in the Gal-axy, there remains a dearth of recognized metal-poor giants in the solar neighborhood, particularly those located close to the Galactic plane. Indeed, until quite recently it was assumed that the metallicity distribution function of the thick disk component of the Galaxy cut off rather sharply below [Fe/H] ≈ −1, hence the only expected contributor to a local metal-weak population of giants would be the extremely low density halo population. Even if one takes the view that such metal-weak stars might exist in the solar

neighborhood, there are clear reasons why they might have been heretofore overlooked: (1) The selection criteria for most surveys of (nonkinematically selected) metal-poor stars begins by concentrating on areas of the sky above Galactic latitude $|b| = 30°$, so as to minimize the number of spurious candidates included from the more metal-rich (and much higher density) disk populations (thick and thin); (2) recent objective-prism surveys have concentrated on fainter targets, and generally saturate at brighter apparent magnitudes; and (3) although one might have hoped to find nearby (bright) metal-poor stars among high proper motion catalogs, if a significant fraction of local metal-weak stars possess kinematics of a disklike population, they will have been selected against in these catalogs. Even when one considers high Galactic latitudes, there does not exist a plethora of recognized nearby metal-poor giants. For example, there are only 32 bright giants with $[\mathrm{Fe/H}] \le -2.0$ in the recent study of Burris et al. (2000), essentially all drawn from the objective-prism survey of Bond (1980). The Beers et al. (2000) catalog (based on a compilation of numerous sources) lists only 75 giants with $[\mathrm{Fe/H}] \le -2.0$ and with $V \le 12.0$.

The detection of relatively nearby metal-poor stars would make up a useful sample for many investigations. For example, metal-poor stars near the disk plane are a priori much more likely to be members of the metal-weak thick disk (hereafter MWTD) population,[3] which several authors have argued includes stars as metal-deficient as $[\mathrm{Fe/H}] \sim -1.6$ (Norris, Bessell, & Pickles 1985; Morrison, Flynn, & Freeman 1990; Morrison 1993; Beers & Sommer-Larson 1995; Layden 1995; Martin & Morrison 1998; Chiba, Yoshii, & Beers 1999; Katz et al. 1999; Chiba & Beers 2000) and perhaps even lower. One of the motivations for the present work was to test whether the relative fraction of MWTD stars in a sample of bright metal-poor giants located near the Galactic plane might be substantially higher than previously claimed, owing to the low-latitude cutoffs of most kinematically unbiased surveys.

The general pattern of relative elemental abundances for stars thought to be members of the MWTD population is still poorly known, although recent efforts are improving the situation (Fuhrmann 1998; Bonifacio, Centurion, & Molaro 1999; Mashonkina & Gehren 2000; Prochaska et al. 2000). Because of their lower temperatures, metal-deficient giants have much richer absorption-line spectra than their warmer main-sequence counterparts, providing the opportunity to study many more elemental species (e.g., Burris et al. 2000; Norris, Ryan, & Beers 2001). In addition, with the completion of the *Hipparcos* mission (ESA 1997) and the recently released Tycho II catalog (Høg et al. 2000), many stars brighter than $V \sim 12$ now have accurately measured proper motions, allowing for the derivation of full space motions, once radial velocities are obtained and distance

estimates are made. Clearly, efforts to increase the number of recognized bright metal-poor giants are important.

The original Case-Hamburg OB star surveys (see Stephenson & Sanduleak 1971, and references therein) primarily concentrated on Galactic latitudes within the relatively narrow region $-10° \le b \le +10°$. The Luminous Stars Extension (LSE) survey of Drilling & Bergeron (1995) sought to detect additional OB stars (in particular, extreme helium stars and very hot OB subdwarfs) by extending the original Case-Hamburg surveys to cover the Galactic latitude range $b = \pm 10°$ to $\pm 30°$ in the Galactic longitude interval $-60° \le l \le +60°$[4]. In the course of this effort, a number of apparently metal-deficient late-type stars, most of which were expected to be giants, were noted in the process of visual inspection of the objective-prism plates.

In this paper, we report new medium-resolution (1–2 Å) spectroscopy for all 39 candidate metal-poor giants from the LSE survey, and, for the majority of the sample, newly measured broadband *UBV* photometry. In § 2, we describe the acquisition of the spectroscopy, the measurement of radial velocities and line-strength indices, the newly obtained broadband photometry, and reddening and distance estimates. Estimation of reddening is more important for the present sample of stars than for stars with $|b| > 30°$, owing to the generally higher values of color excess and the increase in the patchiness of interstellar dust and gas at lower latitudes. As such, we seek to find consistency between estimates of dereddened colors that make use of measured photometry and independent estimates of dereddened color from a newly defined Balmer line index. We then apply several separate approaches to obtain estimates of the metallicities of our program stars, including the calibration of Beers et al. (1999), a newly calibrated artificial neural network (hereafter ANN) approach based on line index information, and a previously calibrated ANN approach (Snider et al. 2001) that makes use of the full set of input pixels of each program spectrum. In § 3, we report *Hipparcos* and Tycho II proper motions and describe the derivation of space motions for the LSE stars. We then consider the kinematics of the LSE giants, in particular their rotational velocities, and compare them with those of other bright metal-poor giants with space motions provided by Chiba & Beers (2000). The distribution of derived orbital eccentricities is then used to consider the fraction of MWTD stars that are represented in this new sample. A summary of our results, and a discussion of their implications are presented in § 4.

2. SPECTROSCOPY, RADIAL VELOCITIES, PHOTOMETRY, AND DISTANCE ESTIMATES

2.1. *Spectroscopic Measurements and Data Reduction*

The LSE metal-deficient candidates observed in our program (designated as " MD? " in the original spectroscopic classifications of Drilling & Bergeron 1995) are provided in Table 1. Column (1) lists the star name. Columns (2) and (3) list the (J2000.0) equatorial coordinates of the stars. The Galactic longitude and latitude for each star is listed in columns (4) and (5), respectively. The approximate *V*- or *B*-

---

[3] It remains unclear whether the MWTD (with a low-metallicity tail extending down to at least $[\mathrm{Fe/H}] = -1.6$ and, as we argue in this paper, probably lower) is properly considered a separate population from the canonical thick disk (with a metallicity distribution function peaking around $[\mathrm{Fe/H}] \sim -0.6$), or whether it is, in reality, the metal-weak tail of this same population; for simplicity of the nomenclature, we refer to the MWTD as an individual population, although we hope to address its relationship to the canonical thick disk based on new and more extensive surveys in the near future.

---

[4] A portion of this range was intersected by plates taken in connection with the LS IV survey; these regions were *not* inspected. See Fig. 1 of Drilling & Bergeron (1995).

TABLE 1
Positions, Velocities, and Line Indices for LSE Stars

Star (1)	R.A. (J2000.0) (2)	Decl. (J2000.0) (3)	l (4)	b (5)	GSC (6)	Source[a] (7)	Vel. (8)	H8 (9)	KP (10)	HP2 (11)	CAP (12)	GP (13)	HG2 (14)	LACF (15)	Other (16)
LSE 90	13 28 07.4	−35 51 53	311.2	26.4	11.6 B	E1	−1	1.67	7.20	1.14	0.43	2.01	1.45	−0.34	. . .
LSE 92	13 46 03.5	−33 56 27	315.7	27.6	10.7 B	E1	398	2.30	9.91	0.90	0.49	5.18	1.28	0.18	CD −33°9314
LSE 97	13 59 17.7	−36 32 52	317.8	24.4	11.1 B	E3	127	1.42	8.32	0.61	0.43	2.45	0.87	−0.38	CD −35°9167
LSE 112	12 57 40.9	−40 39 18	304.2	22.2	11.5 B	E3	−18	0.82	10.16	0.79	0.37	5.42	0.98	0.31	. . .
LSE 113	12 53 57.4	−38 01 36	303.5	24.8	11.6 B	C4	98	2.43	7.62	1.84	0.91	3.96	1.71	−0.13	CD −37°8219
LSE 118	14 51 51.9	−39 59 07	326.7	17.3	11.9 B	E3	−99	1.51	6.47	0.65	0.25	2.31	0.82	−0.50	. . .
LSE 129	17 35 34.8	+15 27 20	38.8	23.6	10.6 V	C4	7	2.10	9.29	2.67	0.51	4.35	2.58	0.42	. . .
LSE 131	17 43 12.2	+12 26 09	36.7	20.7	11.1 V	E1	20	1.95	4.20	1.22	0.34	2.89	1.36	−0.40	. . .
LSE 138	18 24 41.2	+17 24 52	45.8	13.6	12.2 V	C4	11	5.29	5.42	6.92	0.70	1.65	7.07	0.47	. . .
LSE 144	18 32 48.2	−34 22 08	0.0	−11.4	9.9 B	C4	4	. . .	9.89	0.73	0.38	5.68	0.54	0.49	CD −34°12904
LSE 145	18 29 47.5	−34 29 33	359.6	−10.9	10.3 B	C4	143	2.25	8.70	1.72	0.66	3.65	1.65	0.18	. . .
LSE 149	19 37 11.9	−39 44 37	359.4	−25.3	9.1 B	C4	98	1.61	7.64	0.82	0.56	2.65	0.84	−0.03	HD 184711
LSE 150	12 45 53.6	−43 34 04	301.9	19.3	12.3 B	E3	49	3.16	8.40	3.47	0.56	3.47	3.34	0.20	. . .
LSE 151	12 57 16.7	−43 35 32	304.1	19.3	10.7 B	E1	128	2.08	9.28	1.00	0.31	4.85	1.29	−0.02	CD −42°8003
LSE 152	13 44 36.7	−41 43 16	313.5	20.1	11.4 B	E1	−30	2.09	7.62	0.99	. . .	4.47	1.38	−0.12	. . .
LSE 155	14 42 55.6	−45 14 24	322.7	13.3	12.1 B	E1	−112	2.22	9.00	1.64	0.64	3.52	1.86	0.19	. . .
LSE 156	14 53 33.1	−44 28 30	324.8	13.2	11.6 B	E1	52	1.47	6.63	1.17	0.41	2.12	1.29	−0.23	. . .
LSE 157	15 26 43.1	−42 18 37	331.2	11.9	11.1 B	E3	−41	0.50	9.28	1.07	0.30	5.18	1.12	0.29	. . .
LSE 164	18 20 35.1	+24 15 50	51.9	17.2	10.8 V	E1	−196	1.04	5.64	0.97	0.47	2.86	1.80	−0.12	. . .
LSE 173	18 27 23.8	−43 42 41	350.8	−14.3	11.5 B	C4	33	1.94	8.10	1.38	0.48	1.89	1.45	−0.11	. . .
LSE 182	19 10 36.9	−43 16 36	354.2	−21.5	9.8 B	C4	343	2.20	7.74	1.65	0.43	1.97	1.55	−0.20	HD 178443
LSE 184	19 31 18.4	−44 23 26	354.1	−25.4	11.0 B	C4	−162	1.59	8.20	1.25	0.57	1.96	1.42	0.02	HD 183393
LSE 185	19 39 19.1	−44 25 30	354.5	−26.8	11.2 B	E3	−129	. . .	10.05	0.45	0.52	4.25	0.80	−0.06	. . .
LSE 189	19 43 02.3	−51 05 16	347.2	−28.7	11.8 B	E1	−196	1.48	8.97	0.64	0.68	3.38	1.27	−0.07	. . .
LSE 192	14 13 56.4	−38 05 46	320.3	22.0	11.1 B	E3	231	1.69	9.14	0.62	0.83	3.30	0.94	0.37	CD −37°9248
LSE 193	17 56 16.1	+26 37 04	52.1	23.2	10.1 B	E1	−327	2.00	8.76	0.93	0.61	4.64	1.39	0.40	BD +26°3126
LSE 195	18 27 26.3	+28 18 36	56.4	17.4	10.9 V	E3	−48	1.28	10.07	0.81	0.26	5.59	0.61	0.36	. . .
LSE 197	18 49 22.4	+27 48 22	57.9	12.7	9.0 V	E1	−274	1.31	10.43	0.73	0.68	5.26	1.04	0.27	HD 336969
LSE 202	17 58 28.3	+30 31 12	56.3	24.0	10.7 V	E1	−384	1.47	5.78	0.81	0.63	3.19	1.50	0.00	. . .
LSE 205	16 32 25.1	−84 25 55	307.9	−23.9	9.8 B	C4	192	1.87	8.71	0.94	0.67	2.76	1.08	0.00	CPD −84°522
LSE 215	16 39 48.2	−73 01 47	317.8	−17.2	10.8 B	C4	253	1.31	8.74	0.82	0.66	3.43	0.74	0.13	CD −72°1253
LSE 218	16 34 56.5	−70 06 22	319.9	−15.0	10.3 B	E1	114	2.14	8.39	0.85	0.25	4.58	1.35	0.03	CD −69°1546
LSE 228	15 35 48.0	−69 07 05	316.7	−10.8	10.6 B	C4	12	3.54	8.36	3.98	0.71	3.01	4.06	0.30	HD 138300
LSE 232	16 44 11.1	−66 38 49	323.2	−13.5	11.1 B	E1	73	1.06	8.17	0.46	0.74	3.38	1.18	−0.02	. . .
LSE 235	18 54 24.8	−65 29 38	330.1	−24.8	11.3 B	C4	−25	2.09	8.91	1.81	0.47	5.05	1.81	0.44	. . .
LSE 241	18 20 55.7	−61 50 27	332.8	−20.3	10.6 B	C4	153	1.45	7.19	0.77	0.53	2.13	0.83	−0.18	CD −61°5981
LSE 245	17 40 06.8	−61 02 13	331.5	−15.5	10.9 B	E1	267	1.67	7.83	1.01	0.51	3.95	1.24	−0.26	CD −60°6745
LSE 247	17 05 32.3	−62 24 09	328.1	−12.7	10.8 B	E1	6	1.72	9.40	1.12	0.55	4.40	1.42	0.09	. . .
LSE 266	17 52 14.8	−53 17 22	339.4	−13.3	10.7 B	E1	189	2.08	7.48	0.92	0.34	1.91	1.39	−0.16	CD −53°7436

Note.—Units of right ascension are hours, minutes, and seconds, and units of declination are degrees, arcminutes, and arcseconds.
[a] The telescopes are as follows: (C4) CTIO 4 m; (E1) ESO 1.5 m; (E3) ESO 3.6 m.

band apparent magnitude, as provided in the *HST* Guide Star Catalog (Morrison et al. 1996), is listed in column (6), with the appropriate band noted.

Most of the LSE candidates were observed as "fillers" during other spectroscopic campaigns, when conditions were less than optimal for the primary program. As a result, the medium-resolution (1–2 Å over 2 pixels) spectroscopy reported in this paper has been obtained using a number of telescopes and instrumentation. Table 2 lists the telescopes, detectors, wavelength coverage, dispersion of the spectra, and the numbers of stars observed with each combination of equipment. The source of the spectroscopic data for each star is indicated by the code in column (7) of Table 1.

The LSE stars were typically observed to a minimum signal-to-noise (S/N) ratio of approximately 20 : 1 at 4000 Å. In a number of cases, much higher S/N spectra were obtained. Spectra of calibration arc lamps were obtained before or after each program star, and nightly flat fields and

bias frames were taken. Data reduction followed standard procedures using the IRAF[5] suite of routines as described in Beers et al. (1999). Figure 1 shows several example spectra of metal-deficient LSE candidates with similar colors, arranged from relatively metal-rich to relatively metal-poor.

2.2. *Measurement of Radial Velocities and Line Indices*

Radial velocities were measured for each of our program stars using the line-by-line and cross-correlation techniques described in detail by Beers et al. (1999) and references therein. The spectral resolution is similar to that obtained for the majority of the HK survey follow-up, hence we

Telescope	Spectrograph/Detector	Coverage (Å)	Dispersion (Å pixel^{-1})	Number
CTIO 4 m........	RC Spectrograph + Tek 2048 × 2048	3750–5000	0.50	14
ESO 1.5 m.......	Boller & Chivens + Ford/Loral 2048 × 2048	3750–4750	0.65	17
ESO 3.6 m.......	EFOSC2 + Loral 2048 × 2048	3400–5100	1.00	8

anticipate that the measured radial velocities should be accurate to the same level, on the order of 7–10 km s^{-1} (1 σ). Comparison with radial velocities for standard stars observed during the same campaigns during which our program was conducted (and with similar S/N values as our program objects) indicate that this accuracy was indeed achieved. A few of these stars have had high-resolution measurements obtained during the course of the Cayrel et al. Large Programme with VLT/UVES—all velocities are consistent within the above quoted 1 σ error. Measurements of heliocentric radial velocities, after correction for the Earth's rotation and orbital motion, are listed in column (8) of Table 1. Published radial velocities, based on high-

Fig. 1.—Example spectra of four LSE giants with similar dereddened colors and with metallicities obtained as described in the text, arranged from relatively metal-rich to relatively metal-poor. The spectra have been normalized to a continuum approximately equal to unity and shifted to zero rest velocity. Note that the original spectra extended redder than shown; the region depicted in the figure is meant to emphasize the metallic features that drive the metallicity estimates.

resolution spectroscopy for two of our stars, provide additional confidence that our velocity measurements are within the expected errors. For LSE 149 (HD 178443), Bond (1980) obtained $V_{rad} = 102$ km s^{-1}, which differs by only 4 km s^{-1} from the value reported in Table 8. For LSE 182 (HD 184711), McWilliam et al. (1995b) report $V_{rad} = 343$ km s^{-1}, identical to the value reported in Table 8.

For each star, the derived (geocentric) radial velocities were used to place a set of fixed bands for the derivation of line-strength indices, which are pseudo–equivalent widths of prominent spectral features. The bands we employ are summarized in Table 3. A complete discussion of the choice of bands and the "band switching" scheme used to produce our derived Ca II K line index, KP, and the Balmer line index, HP2, which measures the strength of the Hδ line, is provided in Beers et al. (1999). The additional Balmer line index, HG2, is a band-switched measurement of the strength of the Hγ line and is defined in a completely analogous manner to HP2.

Line indices (in angstroms) for prominent spectral features for each of the program stars are reported in columns (9)–(14) of Table 1. Based on repeated measurements of numerous standard stars, our expectation is that, for a spectrum of reasonably good S/N ratio (S/N = 20 or more), errors in the line indices on the order of 0.1 Å are achieved. In order for a line index measurement to be considered a detection, we require that the derived indices be above a minimum value of 0.25 Å. Indices that failed to reach this minimum value are indicated in the table as missing data.

In addition to the line-strength indices, we have measured an autocorrelation function (ACF) index for each spectrum, as described in detail in Beers et al. (1999). We actually make use of the base-10 logarithm of this index, hence it is referred to as LACF. The LACF index quantifies the strength of the multitude of weak metallic lines that are present in each spectrum and provides an additional indicator of the overall abundance. It is of particular use for cooler stars, such as many of those in the present program, where the primary metallicity indicator we employ (the Ca II K line KP index) approaches saturation for stars with [Fe/H] > -1.0. The LSE spectra were obtained with a variety of resolutions, hence appropriate correction factors were applied to bring them onto a common system. The calibration procedure of Beers et al. (1999) obtains an optimum metallicity estimate by consideration of both the KP index and the LACF index at a given color. As described below, we also make use of the LACF in the training of ANNs to derive metallicity estimates.

2.3. Broadband UBV Photometry and Reddening Estimation

2.3.1. Newly Obtained UBV

Previously unpublished UBV photometry for 20 of our 39 targets was obtained with the 0.9 m telescope at Cerro Tol-
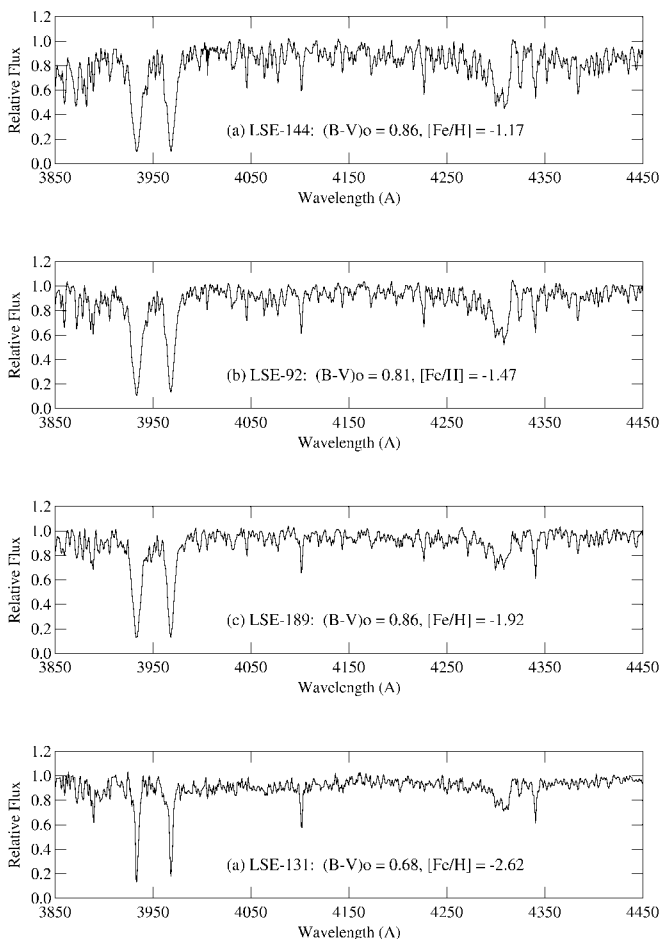
TABLE 3
Line Index Wavelength Bands

Line	Line Band (Å)	Blue Sideband (Å)	Red Sideband (Å)	Band Name
H8..................	3883.1–3895.1	3852.0–3872.0	4000.0–4020.0	H8
Ca II K6..........	3930.7–3936.7	3903.0–3923.0	4000.0–4020.0	KP
Ca II K12........	3927.7–3939.7	3903.0–3923.0	4000.0–4020.0	
Ca II K18........	3924.7–3942.7	3903.0–3923.0	4000.0–4020.0	
Hδ HD12	4095.8–4107.8	4000.0–4020.0	4144.0–4164.0	HP2
Hδ HD24	4089.8–4113.8	4000.0–4020.0	4144.0–4164.0	
Ca I	4214.7–4238.7	4144.0–4164.0	4247.0–4267.0	CAP
G band...........	4297.5–4312.5	4247.0–4267.0	4362.0–4372.0	GP
Hγ HG12.......	4334.5–4346.5	4247.0–4267.0	4415.0–4435.0	HG2
Hγ HG24.......	4328.5–4352.5	4247.0–4267.0	4415.0–4435.0	

olo Inter-American Observatory (CTIO) on the nights of 1980 July 10, 11, and 13, using a standard photoelectric photometer and filters. The reduction procedure outlined by Schulte & Crawford (1961) was used, adopting the following mean extinction coefficients: $k = 0.15$, $k_1 = 0.10$, $k_2 = -0.03$, $k_3 = 0.32$, and $k_4 = 0.00$. Dead times, transformation coefficients, and night corrections were determined from 55 observations of standard stars for which magnitudes and colors are given by Johnson (1963), Johnson et al. (1966), and Landolt (1973). These stars were observed over the same range in color, air mass, and declination as our program stars. Any systematic differences are small compared to the random mean errors: $\sigma V = 0.014$ mag, $\sigma(B-V) = 0.011$ mag, and $\sigma(U-B) = 0.016$ mag, respectively, for a single observation.

Table 4 lists the new photometry, as well as photometry reported in the SIMBAD database and taken from the Tycho II catalog. There are 12 stars in Table 4 for which photometry was obtained from the SIMBAD database, and seven stars for which photometry was taken from the Tycho II catalog. Note that the errors in the Tycho II photometry can become quite large (greater than 0.15 mag) for the stars with $V > 10.5$ (Høg et al. 2000), so improved photometry should be obtained for these stars in the near future. Note, however, that for stars with colors $(B-V)_0 \geq 0.7$, the dependence of two of the metallicity indicators we employ (the KP and LACF indices) on the measured color is not very strong, so modest errors in the derived colors can be tolerated. Nevertheless, as described below, we carry out several checks on the appropriate colors to apply in subsequent analysis of this data. Also note that, as addressed below, the trained ANNs make use exclusively of spectral information and hence are not subject to metallicity errors arising from poor photometry.

2.3.2. Reddening and Distance Estimates

Because the LSE metal-poor candidates all have $|b| < 30°$, careful attention must be paid to the reddening corrections. We initially adopted the Schlegel, Finkbeiner, & Davis (1998) estimates of reddening listed in column (2) of Table 5. The Schlegel et al. estimates have superior spatial resolution and are thought to have a better determined zero point than the Burstein & Heiles (1982) maps. However, Arce & Goodman (1999) caution that the Schlegel et al. map may overestimate the reddening values when their reported color excess, $E(B-V)_S$, exceeds about 0.15 mag. Our own independent tests suggest that this problem may extend to even lower color excesses, on the order of

$E(B-V)_S = 0.10$ mag. Hence, we have adopted a slight revision of the Schlegel et al. reddening estimates, according to the following:

$$E(B - V)_A = \begin{cases} E(B - V)_S , & E(B - V)_S \leq 0.10 , \\ 0.10 + 0.65[E(B - V)_S - 0.10] , \\ & E(B - V)_S > 0.10 , \end{cases} \quad (1)$$

where $E(B-V)_A$ indicates the adopted reddening estimate. We note that for $E(B-V)_S \geq 0.15$ this approximately reproduces the 30%–50% reddening reduction recommended by Arce & Goodman (1999). To account for stars that are located within the reddening layer, assumed to have a scale height $h = 125$ pc, the reddening to a given star at distance D is reduced compared to the total reddening by a factor $[1 - \exp(-|D \sin b|/h)]$.

Distances to individual stars are estimated from M_V versus $(B-V)_0$ relations, as described in Beers et al. (2000). The procedure must be iterated, because both V_0 (and therefore D) and $(B-V)_0$ depend on the adopted reddening. Since the M_V versus $(B-V)_0$ relations depend on metallicity, as well as on the classification of the star, at each step of the iteration, the metallicity is recomputed and the classifications redetermined with the current estimates of $(B-V)_0$ and $(U-B)_0$, so that at the end we obtain consistent estimates of the final reddening, $E(B-V)_F$, D, and [Fe/H]. Based on the work of Beers et al. (2000), we estimate that these distances should be accurate to approximately 10%–20%, although in cases of highly reddened individual stars, they may exceed 20%. We consider the impact of distance errors on the derived kinematics of our program stars in § 3.2 below.

Fortunately, we are not required to rely solely on photometric estimates of the intrinsic colors and reddening, as the line strengths of the observed Balmer lines also provide a means by which a dereddened color may be derived. To implement these estimates, we have trained an ANN (using the commercially available "BackPack 4.1" routine),[6] taking as inputs the base-10 logarithm of the mean Balmer line index, log [(HP2 + HG2)/2] (which we refer to as LDGP below), the logarithm of the KP index (LKP), and the logarithm of the ACF (LACF) and producing as output an estimate of the intrinsic color, which we refer to as BV_{ANN}. For general comments about the use of ANNs for problems of this sort, see the extensive discussion in Snider et al. (2001).

---

[6] From http://www.Zsolutions.com.

TABLE 4
AVAILABLE *UBV* PHOTOMETRY OF LSE STARS

Star	V	$B-V$	$U-B$	Source[a]
LSE 90	10.90	0.79	0.26	P
LSE 92	9.96	0.79	0.20	P
LSE 97	10.26	1.07	0.64	P
LSE 112	10.73	0.87	...	S
LSE 113	10.95	0.83	0.22	P
LSE 118	11.67	0.92	...	T
LSE 129	10.56	0.53	...	S
LSE 131	10.92	0.87	0.22	P
LSE 138	12.30	0.50	0.22	P
LSE 144	9.99	0.87	0.39	P
LSE 145	10.41	0.74	0.18	P
LSE 149	7.99	1.31	0.94	P
LSE 150	11.68	0.78	...	T
LSE 151	10.45	0.86	0.24	P
LSE 152	10.65	0.77	0.11	P
LSE 155	11.32	0.75	0.23	P
LSE 156	10.93	0.95	0.41	P
LSE 157	11.00	0.80	...	T
LSE 164	11.01	0.76	0.07	P
LSE 173	10.71	1.11	0.55	P
LSE 182	10.04	0.65	...	S
LSE 184	10.34	0.75	...	T
LSE 185	10.40	0.80	...	S
LSE 189	11.15	0.87	0.35	P
LSE 192	9.05	1.14	...	S
LSE 193	8.59	0.76	0.11	P
LSE 195	11.26	0.83	0.30	P
LSE 197	9.21	0.89	0.33	P
LSE 202	10.66	0.83	0.25	P
LSE 205	9.86	0.93	...	S
LSE 215	10.45	0.95	...	T
LSE 218	10.11	0.76	...	S
LSE 228	10.26	0.48	...	S
LSE 232	10.42	1.18	...	S
LSE 235	10.99	0.74	...	T
LSE 241	9.68	1.08	...	S
LSE 245	10.25	0.78	...	S
LSE 247	9.99	0.82	...	S
LSE 266	10.45	0.86	...	T

[a] The photometry sources are as follows: (P) present paper; (S) SIMBAD database; (T) Tycho II catalog.

The training of the color estimation ANN was carried out using the subset of 398 of the 551 "standard stars" described by Beers et al. (1999) for which measures of all three inputs were available, setting aside 20% of this sample for use as a validation set to estimate errors in the procedure. Experiments with the number of hidden nodes indicated that minimum errors were obtained with the use of no more than six hidden nodes arranged in a single layer.[7] The overall 1 σ error in prediction of $(B-V)_0$ obtained over the color range $0.3 \leq (B-V)_0 \leq 1.2$ was $\sigma(B-V)_0 = 0.054$

---

[7] In an ANN with a single hidden layer, such as presented here, each node in the hidden layer receives the normalized sum of the weighted inputs, $N^{-1} \sum w_{ij}$ input$_i$. Each hidden node performs a nonlinear operation on its input, allowing the input data to be transformed to a set of nonlinear parameters, the number of which is equal to the number of hidden nodes. These parameters, the outputs of the hidden nodes, are then multiplied by the weights, summed, and normalized, at which point the result of the ANNs is the desired physical parameter, or classification, of a given star. The training procedure is an iterative process of automatically adjusting the weights to minimize the classification error.

mag, with a median offset in estimated color of +0.004 mag. Note, however, that the size of the estimated errors is rather different in the color ranges $0.3 \leq (B-V)_0 \leq 0.8$ and $0.8 < (B-V)_0 \leq 1.2$. For the bluer stars, a prediction error of $\sigma(B-V)_0 = 0.047$ mag was achieved, while for the redder stars, the errors degraded to $\sigma(B-V)_0 = 0.122$ mag. For both ranges, the median color offsets remained small, on the order of 0.003 mag. Estimates of dereddened $(B-V)_0$ colors obtained by the ANN approach, BV_{ANN}, are listed in column (8) of Table 5.

For convenience, in Table 5 we have also listed the measured $B-V$ colors and their sources in columns (2) and (3), respectively. Column (4) lists the initial reddening from Schlegel et al. (1998), $E(B-V)_S$, while column (5) lists the adopted initial reddening, after reduction in some cases as described above, $E(B-V)_A$. The first-pass distance-corrected estimate of reddening obtained from the iterative procedure described above, $E(B-V)_F$, is listed in column (6); the resulting first-pass dereddened color $(B-V)_0$ is listed in column (7). Comparison of the first-pass dereddened colors in column (7) with the ANN estimates listed in column (8) reveals general agreement, at least for stars with measured dereddened colors $(B-V)_0 \leq 1.0$. For the 17 stars in this color range with photometry in which we have the greatest confidence (listed as source "P"), the median offset in $BV_{ANN} - (B-V)_0$ is -0.050 mag, with a 1 σ scatter between the two estimates of dereddened color of $\sigma = 0.067$ mag. For the 17 stars for which photometry is drawn from either the SIMBAD database or the Tycho II catalog, which are likely to have larger errors, the median offset between the dereddened color estimates in this same range of color is -0.010 mag, with a 1 σ scatter of $\sigma = 0.074$ mag.

There is no guarantee that the final Schlegel et al. estimates of reddening listed in column (6) of Table 5 are themselves correct, so we have decided to proceed, for stars with $(B-V)_0 \leq 1.0$, using a straight mean of the two estimates of dereddened color listed in columns (7) and (8). The mean value of estimated dereddened color is listed in column (9) and is designated $\langle (B-V)_0 \rangle$. Since, for stars with $(B-V)_0 > 1.0$, the LDGP index is quite small and subject to greater observational errors reflecting the weakness of the Balmer lines upon which it is based, we are concerned about the accuracy of the listed BV_{ANN} estimates for a few of the program stars. In these cases, we have simply adopted the value obtained from the photometric estimate listed in column (7). One can then define an "effective reddening," $E(B-V)_E = (B-V) - \langle (B-V)_0 \rangle$, which we list in column (10) of Table 5. In some cases, this effective reddening is less than zero, due to possible errors in the reported colors of stars for which we have not obtained measured photometry of our own.

We proceed with the type classifications, estimated absolute magnitudes, and associated distance estimates, carried out according to the procedures described by Beers et al. (2000), based on our best estimates of dereddened colors, $\langle (B-V)_0 \rangle$, and reddening, $E(B-V)_E$, as obtained above. The assigned classification of each star is listed in column (11) of Table 5. Columns (12) and (13) list the adopted absolute magnitude and distance estimates, respectively.

2.4. *Metallicity Estimates*

Much of the past debate concerning the reality of the MWTD has centered around the validity of estimated stel-

TABLE 5
DERIVED REDDENINGS, CLASSIFICATIONS, ABSOLUTE MAGNITUDES, AND DISTANCES

Star (1)	$B-V$ (2)	Source (3)	$E(B-V)_S$ (4)	$E(B-V)_A$ (5)	$E(B-V)_F$ (6)	$(B-V)_0$ (7)	BV_{ANN} (8)	$\langle (B-V)_0 \rangle$ (9)	$E(B-V)_E$ (10)	Type[a] (11)	M_V (12)	Dist. (pc) (13)
LSE 90	0.79	P	0.069	0.069	0.05	0.74	0.68	0.71	0.08	G	0.94	404
LSE 92	0.79	P	0.051	0.051	0.02	0.77	0.78	0.78	0.01	G	2.19	200
LSE 97	1.07	P	0.077	0.077	0.05	1.02	0.95	1.02	0.05	G	−1.81	337
LSE 112	0.87	S	0.139	0.125	0.07	0.80	0.83	0.81	0.06	G	1.95	261
LSE 113	0.83	P	0.072	0.072	0.05	0.78	0.60	0.69	0.14	G	1.71	347
LSE 118	0.92	T	0.108	0.105	0.10	0.82	0.90	0.86	0.06	G	−0.80	1335
LSE 129	0.53	S	0.076	0.076	0.05	0.48	0.59	0.53	0.00	TO	3.88	217
LSE 131	0.87	P	0.138	0.125	0.12	0.75	0.61	0.68	0.19	G	0.82	728
LSE 138	0.50	P	0.263	0.206	0.19	0.31	0.48	0.40	0.10	FHB	0.94	1619
LSE 144	0.87	P	0.120	0.113	0.03	0.84	0.89	0.86	0.01	G	0.74	235
LSE 145	0.74	P	0.114	0.109	0.04	0.70	0.64	0.67	0.07	G	3.29	234
LSE 149	1.31	P	0.114	0.109	0.05	1.26	0.77	1.26	0.05	G	−3.15	202
LSE 150	0.78	T	0.105	0.103	0.07	0.71	0.53	0.62	0.16	SG	3.62	325
LSE 151	0.86	P	0.103	0.102	0.05	0.81	0.76	0.79	0.07	G	1.48	263
LSE 152	0.77	P	0.089	0.089	0.05	0.72	0.69	0.70	0.07	G	1.60	334
LSE 155	0.75	P	0.162	0.140	0.06	0.69	0.64	0.67	0.08	SG	3.61	311
LSE 156	0.95	P	0.179	0.151	0.10	0.85	0.66	0.76	0.19	G	0.15	382
LSE 157	0.80	T	0.151	0.133	0.05	0.75	0.74	0.74	0.06	G	2.53	307
LSE 164	0.76	P	0.139	0.125	0.08	0.68	0.60	0.64	0.12	G	1.62	411
LSE 173	1.11	P	0.070	0.070	0.04	1.07	0.67	1.07	0.04	G	−2.39	474
LSE 182	0.65	S	0.087	0.087	0.04	0.61	0.63	0.62	0.03	SG	3.51	194
LSE 184	0.75	T	0.082	0.082	0.05	0.70	0.67	0.69	0.06	G	2.14	276
LSE 185	0.80	S	0.070	0.070	0.04	0.76	1.03	0.90	−0.10	G	0.34	337
LSE 189	0.87	P	0.043	0.043	0.03	0.84	0.80	0.82	0.05	G	0.45	430
LSE 192	1.14	S	0.069	0.069	0.03	1.11	0.81	0.96	0.00	G	−2.15	190
LSE 193	0.76	P	0.079	0.079	0.02	0.74	0.70	0.72	0.04	G	2.41	112
LSE 195	0.83	P	0.098	0.098	0.05	0.78	0.88	0.83	0.00	G	1.53	382
LSE 197	0.89	P	0.202	0.166	0.03	0.86	0.85	0.85	0.04	G	1.64	131
LSE 202	0.83	P	0.051	0.051	0.04	0.79	0.63	0.71	0.12	G	0.64	371
LSE 205	0.93	S	0.120	0.113	0.06	0.87	0.77	0.82	0.11	G	0.20	226
LSE 215	0.95	T	0.101	0.101	0.06	0.89	0.82	0.85	0.10	G	−0.23	309
LSE 218	0.76	S	0.081	0.081	0.03	0.73	0.72	0.72	0.04	G	1.80	256
LSE 228	0.48	S	0.083	0.083	0.02	0.46	0.52	0.49	−0.01	TO	4.01	180
LSE 232	1.18	S	0.092	0.092	0.05	1.13	0.81	1.13	0.05	G	−2.50	397
LSE 235	0.74	T	0.075	0.075	0.05	0.69	0.63	0.66	0.08	SG	3.51	280
LSE 241	1.08	S	0.106	0.104	0.08	1.00	0.80	1.00	0.08	G	−1.83	515
LSE 245	0.78	S	0.084	0.084	0.04	0.74	0.73	0.73	0.05	G	0.90	303
LSE 247	0.82	S	0.119	0.112	0.04	0.78	0.72	0.75	0.07	G	2.16	201
LSE 266	0.86	T	0.130	0.120	0.06	0.80	0.70	0.75	0.11	G	0.42	325

[a] The stellar type codes are as follows: (FHB) field horizontal branch; (G) giant; (SG) subgiant; (TO) main-sequence turnoff.

lar abundances for putative members of this population (e.g., Twarog & Anthony-Twarog 1994; Ryan & Lambert 1995). Hence, we have endeavored to take particular care in the present study to obtain metallicity estimates from several different approaches. Broadly speaking, we can divide the methods we employ into two categories, "photometric" abundance estimates, which involve the use of line indices and estimates of dereddened $(B-V)_0$ colors, and "nonphotometric" abundance estimates, which make use of line indices or spectral information that *does not* depend on estimates of dereddened colors and thus provides some confidence that a grossly incorrect metallicity is not derived as the result of an incorrectly adopted dereddened color. We have also used a number of different calibrations (all of which are based on subsets of the Beers et al. 1999 standard stars) to ensure that our final results are not dependent on any single calibration. The two sets of estimation procedures are discussed below.

2.4.1. *Estimates Using Estimated Dereddened Colors*

Beers et al. (1999) describe a technique for the estimation of [Fe/H] from medium-resolution spectroscopy of stars based on the strength of the Ca II K line index, KP, and the LACF index, as a function of dereddened $(B-V)_0$ color, with accuracy on the order of 0.15–0.2 dex over the abundance range $-4.0 \leq$ [Fe/H] $\leq +0.3$. This method makes use of an optimal combination of independent estimates obtained from the KP line indices and those obtained from the LACF measurements, based on comparisons with predictions of these quantities from synthetic spectra and colors, constrained by observations of a large set of standards with available external high-quality abundance estimates. In Table 6, we list the results of these calculations. Column (1) lists the star name, while column (2) lists the estimated metallicity obtained by application of the Beers et al. (1999) procedure, [Fe/H]$_{AK2}$, and its associated 1 σ error.

TABLE 6
ESTIMATED METALLICITIES FOR LSE STARS

Star (1)	$[Fe/H]_{AK2}$ (2)	$[Fe/H]_{ANN1}$ (3)	$[Fe/H]_{ANN2}$ (4)	$[Fe/H]_{ANN3}$ (5)	$[Fe/H]_F$ (6)
LSE 90	−2.20 (0.13)	−2.20	−2.04	−2.35	−2.20 (0.20)
LSE 92	−1.43 (0.25)	−1.42	−1.38	−1.67	−1.47 (0.20)
LSE 97	−2.49 (0.11)	−2.66	−2.41	−2.26	−2.46 (0.20)
LSE 112	−1.31 (0.26)	−1.26	−1.35	−0.86	−1.20 (0.20)
LSE 113	−1.90 (0.14)	−1.88	−1.58	(−2.64)	−1.79 (0.20)
LSE 118	−2.70 (0.12)	−2.75	−2.72	−2.28	−2.61 (0.20)
LSE 129	−0.25 (0.15)	−0.32	−0.46	−0.10	−0.28 (0.20)
LSE 131	−2.77 (0.15)	−2.63	−2.61	−2.47	−2.62 (0.20)
LSE 138	−0.11 (0.20)	−0.30	−0.30	−0.03	−0.18 (0.20)
LSE 144	−1.06 (0.28)	−1.11	−1.34	(−0.47)	−1.17 (0.20)
LSE 145	−1.52 (0.19)	−1.25	−1.17	−0.91	−1.21 (0.20)
LSE 149	−2.65 (0.12)	−2.43	−2.14	−2.82	−2.51 (0.20)
LSE 150	−1.26 (0.16)	−1.10	−0.64	−0.38	−0.85 (0.20)
LSE 151	−1.58 (0.22)	−1.81	−1.64	−1.88	−1.73 (0.20)
LSE 152	−1.90 (0.14)	−1.90	−1.91	−1.91	−1.91 (0.20)
LSE 155	−1.38 (0.18)	−1.21	−1.17	−1.09	−1.21 (0.20)
LSE 156	−2.23 (0.13)	−2.31	−2.11	−2.73	−2.35 (0.20)
LSE 157	−1.43 (0.23)	−1.22	−1.31	(−0.44)	−1.32 (0.20)
LSE 164	−2.15 (0.13)	−2.01	−2.11	−2.63	−2.22 (0.20)
LSE 173	−2.25 (0.13)	−2.23	−1.69	−1.49	−1.92 (0.20)
LSE 182	−1.70 (0.16)	−1.71	−1.70	−1.58	−1.67 (0.20)
LSE 184	−1.74 (0.18)	−1.62	−1.63	−1.49	−1.62 (0.20)
LSE 185	−1.64 (0.20)	−2.03	−2.15	−1.65	−1.87 (0.20)
LSE 189	−1.75 (0.19)	−1.99	−1.90	−2.04	−1.92 (0.20)
LSE 192	−1.80 (0.20)	−1.59	−1.50	−1.98	−1.72 (0.20)
LSE 193	−1.39 (0.22)	−1.06	−1.20	(−2.17)	−1.22 (0.20)
LSE 195	−1.19 (0.28)	−1.25	−1.49	−0.78	−1.18 (0.20)
LSE 197	−1.21 (0.27)	−1.39	−1.38	−1.75	−1.43 (0.20)
LSE 202	−2.36 (0.13)	−2.07	−2.13	(−3.00)	−2.19 (0.20)
LSE 205	−1.77 (0.21)	−1.92	−1.81	−1.57	−1.77 (0.20)
LSE 215	−1.70 (0.23)	−1.80	−1.88	−2.08	−1.86 (0.20)
LSE 218	−1.71 (0.19)	−1.67	−1.75	−2.11	−1.81 (0.20)
LSE 228	−0.32 (0.20)	−0.45	−0.41	−0.10	−0.32 (0.20)
LSE 232	−2.39 (0.13)	−2.29	−2.08	−2.66	−2.35 (0.20)
LSE 235	−0.97 (0.21)	−0.79	−0.76	−0.31	−0.71 (0.20)
LSE 241	−2.46 (0.12)	−2.46	−2.35	−2.56	−2.46 (0.20)
LSE 245	−1.90 (0.13)	−2.12	−2.04	(−2.87)	−2.02 (0.20)
LSE 247	−1.50 (0.22)	−1.55	−1.45	−1.39	−1.47 (0.20)
LSE 266	−2.05 (0.15)	−2.11	−2.00	−2.21	−2.09 (0.20)

As an alternative, we have trained an ANN, taking as inputs LKP, LACF, and the dereddened color estimate $(B-V)_0$ and producing as output an estimate of the metallicity [Fe/H]. The training was carried out using the subset of 405 of the 551 "standard stars" described by Beers et al. (1999) for which measures of all three inputs were available, setting aside 20% of this sample for use as a validation set to estimate errors in the procedure. As we found in the ANN prediction of dereddened color, minimum errors for metallicity estimation were obtained with the use of no more than six nodes arranged in a single layer. The overall 1 σ error in prediction of metallicity was $\sigma[Fe/H] = 0.26$ dex, with a median offset of +0.04 dex (note that this prediction error *includes* the errors in the metallicities of the Beers et al. 1999 standards themselves). Division of the validation set into several intervals of color and (known) metallicity did not reveal any large deviations from these error levels over the calibration space. We list the resulting abundance estimates, $[Fe/H]_{ANN1}$, in column (3) of Table 6. Inspection of the comparison between the two "photometric" abundance indicators reveals that agreement is generally excellent, and

in most cases, within the quoted 1 σ error estimate. All of the derived abundances agree within 2 σ. Since the majority of the error in the "photometric" abundance indicators probably arises from difficulties in the proper estimation of the reddening correction, we explore alternative approaches as described below. Once near-IR *JHK* photometry from the final release of the 2MASS point-source catalog (Skrutskie et al. 1997) becomes available, we will be able to predict dereddened $(B-V)_0$ colors with more confidence.

2.4.2. *Estimates Using Spectral Information Only*

We have trained yet another ANN, taking as inputs LKP, LACF, and LDGP and producing as output an estimate of the metallicity [Fe/H]. The training was carried out using the subset of 398 of the 551 standard stars from Beers et al. (1999) for which measures of all three inputs were available, setting aside 20% of this sample for use as a validation set to estimate errors in the procedure. Minimum errors for metallicity estimation were obtained with the use of no more than six nodes arranged in a single layer. The overall 1 σ error in

prediction of [Fe/H] was σ[Fe/H] = 0.29 dex, with a median offset of −0.02 dex. Division of the validation set into several intervals of LDGP and (known) metallicity did not reveal any large deviations from these error levels over the calibration space. We list the resulting abundance estimates, [Fe/H]$_{ANN2}$, in column (4) of Table 6.

Snider et al. (2001) describe a procedure for the use of ANNs that take as inputs the entire set of spectral information (after normalization of the spectral energy distribution) over the (minimum) wavelength range 3850–4450 Å and produce as output an estimate of [Fe/H], with an overall 1 σ scatter of about 0.20 dex. We have attempted to make use of this procedure for the present sample of stars, although we were somewhat hampered by resolution limitations, as described below.

All spectra were first rebinned to the nominal dispersion of the trained ANNs used by Snider et al. (2001), 0.65 Å pixel^{-1}. This was a relatively minor change for the spectra obtained with the CTIO 4 m and ESO 1.5 m but required a rather severe oversampling of the data obtained with the ESO 3.6 m. The spectra were then submitted to the network described by Snider et al. as the "total/full" network, details of which can be found in their paper. This network is based on the subset of 279 stars from Beers et al. (1999) with previously observed high S/N medium-resolution spectroscopy available, with a lower S/N limit of about 40 : 1 (at the red end of the spectra).

The estimated abundances that result from this approach, [Fe/H]$_{ANN3}$, are listed in column (5) of Table 6. As can be seen from inspection of the table, for the most part, the resulting abundances are consistent, within 0.5 dex, with the estimated metallicities based on the other approaches we have employed. In a number of cases, however, the [Fe/H]$_{ANN3}$ did not agree very well. We have indicated these cases in the tables by putting the more doubtful results in parentheses. The reasons for these disagreements may involve a number of sources: (1) Three of the spectra with gross deviations are from the ESO 3.6 m, which, as we commented above, had to be oversampled in order to run them through the previously trained network, and (2) the network used to evaluate our stars is not populated with large numbers of metal-poor giants, and gaps in the coverage of the pertinent ranges of this parameter space may be a limiting factor. Despite these difficulties, the consistency in metallicity estimates obtained for the majority of the program stars from this method, as compared to the other approaches, provides confidence in this technique. It was suggested by an anonymous referee that we consider dropping the [Fe/H]$_{ANN3}$ estimates of abundances in our final averages. We have decided not to follow this advice (except for the problematic cases), on the grounds that these estimates are based on a completely different (albeit new, and less than optimally tested) calibration that, unlike all of our other approaches, does not involve individual line index measurements.

2.4.3. Final Adopted Metallicities and Comparison with Available High-Resolution Abundance Estimates

We obtain our final abundance estimates from a straight average of the four derived abundances for each star listed above—two "photometric" and two "nonphotometric." In the case of the rejected [Fe/H]$_{ANN3}$ estimates, we have simply dropped these from the averaging. The final esti-

mates of metallicity, [Fe/H]$_F$, are listed in column (6) of Table 6. Although we do not have individual 1 σ error estimates for the [Fe/H]$_{ANN3}$ results, the Snider et al. (2001) results lead us to believe that they should be on the order of σ[Fe/H] = 0.2 dex, similar to the errors we were able to obtain from the application of the Beers et al. (1999) calibration. Certainly, the range of values reported in Table 6 from the application of different abundance estimation procedures supports this assumption. A comparison of the average metallicity obtained from the first three estimates listed in Table 6 ([Fe/H]$_{AK2}$, [Fe/H]$_{ANN1}$, [Fe/H]$_{ANN2}$) with the 33 accepted [Fe/H]$_{ANN3}$ estimates indicates the presence of a zero-point offset of only +0.03 dex and a 1 σ scatter of 0.31 dex of [Fe/H]$_{ANN3}$ with respect to the other methods, consistent with expectations.

The use of multiple metallicity estimation procedures relying on different inputs (and different calibrations) will serve to decrease the systematic errors associated with any single method. Ultimately, the errors in our determination of metallicity are driven by the accuracy of the abundances assigned to the Beers et al. (1999) standards, so we conservatively adopt a global (external) error estimate of 0.2 dex to our final abundance estimates.

Among the LSE metal-poor candidates, we have rediscovered the bright metal-poor giant HD 184711 (LSE 149), for which the average abundance reported by Beers et al. (1999), based on high-resolution spectroscopic measurements, is [Fe/H] = −2.51. The agreement with the final abundance reported in Table 6, [Fe/H]$_F$ = −2.52 ± 0.20, is excellent. Another of our program stars, LSE 182, is the bright giant HD 178443, for which McWilliam et al. (1995a) obtained an abundance estimate of [Fe/H] = −2.07. This is somewhat lower than we have assigned, [Fe/H]$_F$ = −1.68 ± 0.20, but only by about 2 σ (disregarding the error in the high-resolution estimate).

Several LSE stars were targeted for high-resolution study as part of a recently completed Large Programme with VLT/UVES by Cayrel et al. These included the most metal-deficient star in the sample, LSE 131 ([Fe/H]$_F$ = −2.62), and two stars of somewhat higher abundance but with kinematics (as discussed below) that suggest possible association with the MWTD, LSE 173 ([Fe/H]$_F$ = −1.92) and LSE 232 ([Fe/H]$_F$ = −2.35). Final abundance estimates from the Cayrel et al. UVES observations have not been obtained as of yet, but preliminary inspection of the high-resolution spectrum for LSE 131 confirms that its abundance is consistent with [Fe/H] ≈ −2.5 or slightly lower. A previous high-resolution spectrum of LSE 131, obtained with the ESO 3.6 m telescope and reported by Spite et al. (1999), suggests an abundance [Fe/H] = −2.8, in close agreement with the estimated abundance obtained in the present paper. We conclude that our abundance estimates should be trusted, and we proceed with our kinematic analysis below.

3. HIPPARCOS AND TYCHO II PROPER MOTIONS AND DERIVED SPACE MOTIONS

Ten stars in the present program were included in the Hipparcos catalog, with average accuracies of 2.43 mas yr^{-1} in $\mu_{\alpha*}$ (=μ_α cos δ) and 1.86 mas yr^{-1} in μ_δ, respectively. Columns (6)–(9) of Table 7 list $\mu_{\alpha*}$, μ_δ, and their associated errors as given in the Hipparcos catalog. All of these same stars, as well as the fainter ones, have proper motions available from the Tycho II catalog, with average accuracies of

TABLE 7
PROPER MOTIONS

Star (1)	$\mu_\alpha*$ (mas yr⁻¹) (2)	$\sigma_{\mu_\alpha*}$ (mas yr⁻¹) (3)	μ_δ (mas yr⁻¹) (4)	σ_{μ_δ} (mas yr⁻¹) (5)	$\mu_\alpha*$ (mas yr⁻¹) (6)	$\sigma_{\mu_\alpha*}$ (mas yr⁻¹) (7)	μ_δ (mas yr⁻¹) (8)	σ_{μ_δ} (mas yr⁻¹) (9)	$\mu_\alpha*$ (mas yr⁻¹) (10)	$\sigma_{\mu_\alpha*}$ (mas yr⁻¹) (11)	μ_δ (mas yr⁻¹) (12)	σ_{μ_δ} (mas yr⁻¹) (13)
LSE 90	−31.1	2.4	−13.3	2.4	...	...	...	...	−31.1	2.4	−13.3	2.4
LSE 92	17.8	1.6	−58.1	1.6	19.74	2.64	−58.99	2.11	18.3	1.4	−58.4	1.3
LSE 97	−7.7	1.6	−0.5	1.6	−7.66	2.02	0.53	1.55	−7.7	1.3	0.0	1.1
LSE 112	−17.9	2.1	−34.5	2.0	...	...	...	...	−17.9	2.1	−34.5	2.0
LSE 113	−26.9	2.5	−58.2	2.5	−34.74	1.99	−56.86	1.60	−31.7	1.6	−57.2	1.3
LSE 118	−38.6	2.6	−23.0	2.5	...	...	...	...	−38.6	2.6	−23.0	2.5
LSE 129	−23.9	1.7	−54.4	1.6	...	...	...	...	−23.9	1.7	−54.4	1.6
LSE 131	−19.5	2.0	−29.3	1.9	...	...	...	...	−19.5	2.0	−29.3	1.9
LSE 138	−1.1	1.7	−14.8	1.7	...	...	...	...	−1.1	1.7	−14.8	1.7
LSE 144	−21.2	1.6	−16.2	1.6	...	...	...	...	−21.2	1.6	−16.2	1.6
LSE 145	−32.1	1.9	−62.0	2.0	...	...	...	...	−32.1	1.9	−62.0	2.0
LSE 149	1.0	1.1	−51.8	1.3	1.42	1.48	−51.12	1.02	1.1	0.9	−51.4	0.8
LSE 150	−4.7	1.9	14.0	1.8	...	...	...	...	−4.7	1.9	14.0	1.8
LSE 151	−15.1	1.4	−1.3	1.3	−9.99	1.06	0.85	0.94	−11.9	0.8	0.1	0.8
LSE 152	−40.9	2.1	−19.8	2.0	...	...	...	...	−40.9	2.1	−19.8	2.0
LSE 155	−60.1	2.2	−20.5	2.1	...	...	...	...	−60.1	2.2	−20.5	2.1
LSE 156	1.2	2.1	1.0	2.0	...	...	...	...	1.2	2.1	1.0	2.0
LSE 157	−3.0	1.7	−10.1	1.6	...	...	...	...	−3.0	1.7	−10.1	1.6
LSE 164	−2.1	1.7	−9.7	1.7	...	...	...	...	−2.1	1.7	−9.7	1.7
LSE 173	5.0	1.8	−2.9	1.7	...	...	...	...	5.0	1.8	−2.9	1.7
LSE 182	−8.0	1.8	−50.8	1.3	−2.46	6.06	−52.58	4.14	−7.6	1.7	−51.0	1.2
LSE 184	−12.6	2.1	−24.9	2.0	...	...	...	...	−12.6	2.1	−24.9	2.0
LSE 185	3.5	2.1	−42.6	2.0	...	...	...	...	3.5	2.1	−42.6	2.0
LSE 189	−11.4	2.7	−18.8	2.5	...	...	...	...	−11.4	2.7	−18.8	2.5
LSE 192	−15.8	1.3	−15.0	1.3	−14.51	1.24	−11.66	0.98	−15.1	0.9	−12.9	0.8
LSE 193	6.7	1.3	29.4	1.2	...	...	...	...	6.7	1.3	29.4	1.2
LSE 195	−11.6	2.4	−20.6	2.4	...	...	...	...	−11.6	2.4	−20.6	2.4
LSE 197	−13.7	1.4	−97.9	1.3	...	...	...	...	−13.7	1.4	−97.9	1.3
LSE 202	−11.6	2.3	−17.8	2.3	...	...	...	...	−11.6	2.3	−17.8	2.3
LSE 205	−18.6	2.0	8.0	1.9	...	...	...	...	−18.6	2.0	8.0	1.9
LSE 215	−9.9	2.7	−6.0	2.5	−7.82	0.96	−10.39	1.58	−8.1	0.9	−9.1	1.3
LSE 218	48.8	2.9	−83.6	2.7	...	...	...	...	48.8	2.9	−83.6	2.7
LSE 228	2.1	2.4	−11.0	2.3	...	...	...	...	2.1	2.4	−11.0	2.3
LSE 232	−12.3	2.5	−25.4	2.4	...	...	...	...	−12.3	2.5	−25.4	2.4
LSE 235	−5.6	1.9	−20.6	2.0	...	...	...	...	−5.6	1.9	−20.6	2.0
LSE 241	−5.4	2.2	−1.6	2.3	−2.86	1.69	−0.36	1.29	−3.8	1.3	−0.7	1.1
LSE 245	−3.7	2.0	−53.1	2.0	...	...	...	...	−3.7	2.0	−53.1	2.0
LSE 247	−31.1	3.5	−15.3	3.3	...	...	...	...	−31.1	3.5	−15.3	3.3
LSE 266	−28.7	3.2	0.8	3.0	−20.56	5.13	−6.37	3.35	−26.4	2.7	−2.4	2.2

2.06 mas yr^{-1} in μ_{α^*} and 1.99 mas yr^{-1} in μ_δ, respectively. Columns (2)–(5) of Table 7 list the proper motions and their associated errors as given in the Tycho II catalog. As in Beers et al. (2000), we construct a variance-weighted average of the available proper motions. These averages, and their associated errors, are listed in columns (10)–(13) of Table 7, respectively.

3.1. *Space Motions for the LSE Stars*

We now derive the space motions and orbital parameters of the LSE stars, following the procedures of Beers et al. (2000); Table 8 provides a summary of the results. Column (1) lists the star name. Column (2) recalls the derived metallicity from Table 6. Columns (3) and (4) list the positions of the stars in the meridional (R, Z)-plane, adopting $R_\odot = 8.5$ kpc as the Galactocentric distance for the Sun. Columns (5)–(7) list the three-dimensional velocities U, V, and W in the directions toward the Galactic anticenter, the rotational

direction, and the north Galactic pole, respectively, along with an estimate of the errors in these quantities that could arise from errors in distance estimates of 20%, as described below. These velocity components are corrected for the solar motion $(U_\odot, V_\odot, W_\odot) = (-9, 12, 7)$ km s^{-1} with respect to the local standard of rest (LSR; Mihalas & Binney 1981). Columns (8) and (9) list the velocity components (V_R, V_ϕ) in the cylindrical rest frame (R, ϕ), respectively, on the assumption that the rotational speed of the LSR around the Galactic center is $V_{LSR} = 220$ km s^{-1}.

To estimate the orbital parameters for these stars, we adopt the analytic Stäckel-type mass model developed by Sommer-Larsen & Zhen (1990), which consists of a flattened, oblate disk and a nearly spherical massive halo. This model reproduces a flat rotation curve beyond $R = 4$ kpc and the local mass density at $R_\odot$, consistent with other observations. Columns (10) and (11) of Table 8 list the estimated apogalactic distances, R_{ap}, and the estimated perigalactic distances, R_{pr}, along the Galactic plane, respectively.

TABLE 8
SPACE MOTIONS AND ORBITAL PARAMETERS

Star (1)	[Fe/H] (dex) (2)	R (kpc) (3)	Z (kpc) (4)	U (km s^{-1}) (5)	V (km s^{-1}) (6)	W (km s^{-1}) (7)	V_R (km s^{-1}) (8)	V_ϕ (km s^{-1}) (9)	R_{ap} (kpc) (10)	R_{pr} (kpc) (11)	Z_{max} (kpc) (12)	e (13)	Population (14)
LSE 90	−2.20	8.27	0.18	34 (11)	−34 (12)	−8 (7)	28	187	8.48	5.97	0.21	0.17 (0.05)	DH[a]
LSE 92	−1.47	8.37	0.09	−283 (8)	−250 (7)	140 (11)	−283	−35	22.16	0.84	11.59	0.93 (0.01)	H
LSE 97	−2.46	8.27	0.14	−86 (7)	−73 (6)	63 (4)	−89	144	9.51	4.05	1.33	0.40 (0.03)	H
LSE 112	−1.20	8.37	0.10	11 (6)	0 (9)	−39 (9)	5	220	8.51	8.24	0.55	0.02 (0.03)	DH[a]
LSE 113	−1.79	8.33	0.15	−35 (7)	−124 (15)	−37 (18)	−38	95	8.49	2.44	0.56	0.55 (0.06)	H
LSE 118	−2.61	7.47	0.40	222 (33)	−176 (50)	−36 (16)	217	65	12.49	1.26	1.25	0.82 (0.14)	H
LSE 129	−0.28	8.35	0.09	−52 (11)	−32 (11)	10 (4)	−49	189	8.99	5.89	0.16	0.21 (0.04)	D
LSE 131	−2.62	7.96	0.26	−90 (14)	−77 (22)	32 (8)	−83	147	8.95	3.91	0.60	0.39 (0.08)	DH
LSE 138	−0.18	7.49	0.38	−99 (20)	−48 (18)	−29 (15)	−72	185	8.68	5.04	0.58	0.26 (0.06)	D
LSE 144	−1.17	8.27	−0.05	−16 (10)	−14 (6)	20 (4)	−16	206	8.41	7.09	0.23	0.09 (0.03)	DH[a]
LSE 145	−1.21	8.27	−0.04	−149 (10)	−66 (16)	−18 (3)	−149	154	11.65	3.71	0.28	0.52 (0.04)	H
LSE 149	−2.51	8.32	−0.09	−91 (9)	−36 (9)	−48 (5)	−91	184	10.19	5.33	0.88	0.31 (0.04)	DH
LSE 150	−0.85	8.34	0.11	−23 (6)	−25 (8)	43 (6)	−29	194	8.64	6.52	0.67	0.14 (0.03)	DH[a]
LSE 151	−1.73	8.36	0.09	−64 (6)	−96 (8)	50 (3)	−67	122	8.94	3.32	0.88	0.46 (0.04)	DH
LSE 152	−1.91	8.29	0.12	57 (12)	−20 (13)	−19 (6)	52	202	9.21	6.39	0.28	0.18 (0.04)	DH[a]
LSE 155	−1.21	8.26	0.07	136 (14)	6 (16)	−9 (4)	131	228	13.68	5.93	0.19	0.40 (0.03)	H
LSE 156	−2.35	8.20	0.09	−52 (8)	−15 (7)	19 (4)	−57	204	9.32	6.32	0.27	0.19 (0.03)	DH[a]
LSE 157	−1.32	8.24	0.06	30 (9)	20 (6)	−11 (4)	26	240	10.00	7.98	0.16	0.11 (0.03)	DH[a]
LSE 164	−2.22	8.26	0.12	91 (7)	−146 (8)	−54 (4)	94	70	9.15	1.73	1.07	0.68 (0.04)	H
LSE 173	−1.92	8.05	−0.12	−37 (10)	6 (4)	−14 (5)	−39	226	9.32	7.28	0.22	0.12 (0.03)	DH[a]
LSE 182	−1.67	8.32	−0.07	−319 (9)	−67 (9)	−126 (4)	−319	153	33.35	3.07	11.66	0.83 (0.01)	H
LSE 184	−1.62	8.25	−0.12	137 (9)	−9 (8)	84 (5)	136	212	13.82	5.74	2.65	0.41 (0.02)	H
LSE 185	−1.87	8.20	−0.15	121 (10)	−41 (13)	47 (7)	120	180	11.08	4.80	0.98	0.40 (0.03)	H
LSE 189	−1.92	8.13	−0.21	160 (9)	8 (10)	116 (8)	157	230	17.43	5.96	5.18	0.49 (0.03)	H
LSE 192	−1.72	8.36	0.07	−165 (7)	−139 (7)	88 (4)	−166	79	11.75	1.94	2.92	0.72 (0.03)	H
LSE 193	−1.22	8.44	0.04	189 (6)	−216 (7)	−120 (4)	189	2	13.00	0.06	5.93	0.99 (0.02)	H
LSE 195	−1.18	8.30	0.11	−18 (9)	−51 (10)	−2 (5)	−12	170	8.33	5.19	0.12	0.23 (0.04)	DH[a]
LSE 197	−1.43	8.43	0.03	81 (12)	−243 (10)	−70 (4)	81	−24	9.06	0.59	1.62	0.88 (0.04)	H
LSE 202	−2.19	8.32	0.15	158 (8)	−303 (9)	−141 (6)	155	−88	12.08	2.80	6.71	0.63 (0.04)	H
LSE 205	−1.77	8.38	−0.09	−118 (6)	−136 (8)	−51 (6)	−120	81	9.92	1.97	1.05	0.67 (0.03)	H
LSE 215	−1.86	8.35	−0.06	−180 (7)	−159 (7)	−67 (3)	−181	58	12.05	1.30	1.89	0.81 (0.02)	H
LSE 218	−1.81	8.31	−0.07	−46 (12)	−70 (7)	−130 (22)	−49	149	8.94	5.57	3.93	0.24 (0.05)	H
LSE 228	−0.32	8.37	−0.03	−14 (7)	2 (7)	−4 (3)	−17	222	8.81	7.93	0.05	0.05 (0.02)	D
LSE 232	−2.35	8.19	−0.09	−33 (11)	−70 (11)	−22 (6)	−37	149	8.40	4.20	0.28	0.33 (0.04)	DH
LSE 235	−0.71	8.28	−0.12	24 (8)	−2 (7)	19 (5)	21	219	8.75	7.68	0.27	0.06 (0.03)	DH[a]
LSE 241	−2.46	8.07	−0.18	−137 (8)	−59 (5)	−38 (5)	−141	157	11.19	3.86	0.80	0.49 (0.03)	H
LSE 245	−2.02	8.24	−0.08	−195 (12)	−168 (12)	−95 (7)	−195	49	12.85	1.15	3.65	0.84 (0.04)	H
LSE 247	−1.47	8.33	−0.04	−2 (9)	−18 (8)	21 (5)	−4	202	8.34	7.05	0.25	0.08 (0.03)	DH[a]
LSE 266	−2.09	8.20	−0.08	−181 (9)	−76 (7)	−3 (8)	−183	141	12.91	3.14	0.13	0.61 (0.03)	H

[a] Indicates likely member of MWTD population.

Column (12) lists the maximum distance above (or below) the plane, $Z_{\max}$, explored by each star in the course of its orbital motion. In column (13), we list the characteristic eccentricities of the orbits, defined as $e = (r_{\mathrm{ap}} - r_{\mathrm{pr}})/(r_{\mathrm{ap}} + r_{\mathrm{pr}})$, where r_{ap} and r_{pr} stand for the apogalactic and perigalactic distances from the Galactic center, respectively.

An anonymous referee suggested that we investigate the impact of possible distance errors on our derived kinematic quantities. We carried out this exercise by repeatedly subsampling from our catalog of program stars, with the listed distances of the stars perturbed by 10%, 20%, and 30%, respectively, then rederiving the quantities UVW and e within our adopted potential. For completeness, we also included the effects of an assumed radial velocity errors of 10 km s^{-1} and the listed errors in the adopted proper motions. The average errors, for the entire set of program stars, obtained from this procedure were as follows:

10% errors in distance: $\langle \epsilon(U, V, W) \rangle = (8, 8, 5)$ km s^{-1},
20% errors in distance: $\langle \epsilon(U, V, W) \rangle = (10, 11, 7)$ km s^{-1},
30% errors in distance: $\langle \epsilon(U, V, W) \rangle = (12, 14, 8)$ km s^{-1},
10%, 20%, 30% errors in distance: $\langle \epsilon(e) \rangle = 0.03, 0.04, 0.05$ km s^{-1}.

Table 8 includes values of the expected errors in the kinematic quantities for individual stars arising from assumed 20% errors in the distance estimates. Note that in all but one case (the most distant star, LSE 118), the likely errors in the derived kinematic quantities are quite small, thus are not expected to significantly affect the interpretation of our results.

3.2. *The Local Fraction of MWTD Stars*

As noted in § 1, previous (nonkinematically biased) searches for metal-deficient stars have concentrated primarily on high Galactic latitudes (the notable exception being MFF90, where the existence of the MWTD was first suggested). This surely has introduced an underestimate of the numbers of nearby MWTD stars, so we were curious to compare the relative fractions of likely MWTD stars in the LSE survey with previous work. As a representative comparison sample, we have selected the 412 giants with $V < 12.0$ and [Fe/H] ≤ -0.6 from the Beers et al. (2000) catalog with available space motions and orbital eccentricities from Chiba & Beers (2000). An anonymous referee pointed out that, by selecting stars from this catalog with available space motions, one runs the risk of unintentionally reintroducing kinematic biases into our comparison sample. Although this certainly is a concern, the original nonkinematical selection of stars in the Beers et al. (2000) sample, from which the Chiba & Beers (2000) catalog was drawn, should minimize this problem. In any event, the inhomogeneous nature of the sample assemblage precludes the possibility of making explicit corrections for possible biases, a fact that should be kept in mind by the reader.

Figures 2a–2c are a plot of the U, V, and W velocity components for the 36 LSE giants and subgiants (*filled circles*) of the present investigation, as well as for the three stars we classify as field horizontal-branch (FHB) or main-sequence turnoff (TO) stars (*open circles*). For the purpose of the kinematic analysis, we have eliminated the one star classified as FHB in Table 5, as well as the two stars classified as TO.

Figures 2d–2f show the same information for the comparison sample described above. It is immediately clear that many of the LSE giants exhibit rather small V velocities, suggesting possible membership in a rapidly rotating population, and small W velocities, suggesting that they are drawn from a population with low vertical velocity dispersion. The distribution of U velocities exhibits a rather high dispersion. This characteristic has been noted in previous samples, but its origin has not yet been satisfactorily explained in the context of present models of Galactic structure, even after attempts to account for selection-related biases (see the discussion of samples considered by Ryan & Norris 1991). The comparison sample of bright giants includes a large number of stars that are clear members of the halo population, as may be inferred from the relatively broad distribution of the individual velocity components below [Fe/H] $= -1.5$.

The derived mean velocities and velocity ellipsoids of the LSE sample and the comparison sample are summarized in Table 9. Although the small numbers of stars limits the accuracy with which the ellipsoid for the LSE stars can be determined, close inspection of these results reveals a few interesting differences between the two samples. First, note that, for the comparison sample, $\langle V \rangle$ changes dramatically, from a moderate velocity lag on the order of -60 km s^{-1} in the metallicity range $-1.6 \le$ [Fe/H] ≤ -0.6 to a velocity lag of roughly -180 km s^{-1} for metallicities below [Fe/H] $= -1.6$. In contrast, the LSE sample exhibits a velocity lag that remains essentially constant, centered around $\langle V \rangle = -80$ km s^{-1} over the different cuts in metallicity. This strongly indicates that the kinematics of the population(s) of stars that the LSE sample are drawn from are rather different from those that are sampled by the comparison sample. Furthermore, note that, at the lowest metallicity cutoff, two of the three components of the LSE sample velocity ellipsoid (σ_V and σ_W) appear significantly lower than the corresponding components of the comparison sample. Interestingly, in the metallicity range $-1.6 \le$ [Fe/H] ≤ -0.6, the σ_U component of the LSE star velocity ellipsoid appears marginally *greater* than the corresponding component of the comparison sample. Again, these results suggests the lack of a common parent population.

The differences between the populations highlighted above can be shown most clearly by contrasting the distribution of V_ϕ for the LSE giants with that of the comparison sample. Figure 3a shows a stripe density plot of V_ϕ for the 34 LSE giants with [Fe/H] ≤ -1.0 (all of which have $|Z| \le 1$ kpc). Figure 3b shows the same diagram for the subset of the 164 giants in the comparison sample with [Fe/H] ≤ -1.0 and $|Z| \le 1$ kpc. Note that, based on the previous discussion of Chiba & Beers 2000, we expect that the comparison sample in this metallicity range may indeed contain a significant number of MWTD stars; these can be seen in Figure 3b as the concentration of lines in the broad velocity interval $150 \le V_\phi \le 250$ km s^{-1}. Of course, this same velocity interval will contain numerous members of the halo population as well because of its large velocity dispersion. Note, however, that the comparison sample *also* contains a large number of stars with velocities we would uniquely associate with the halo population, i.e., $V_\phi < 100$ km s^{-1}. Inspection of Figure 3a suggests that, while the LSE sample certainly contains a handful of halo objects, the concentration of lines in the interval $150 \le V_\phi \le 250$ km s^{-1} is more pronounced than seen in the comparison sample. A
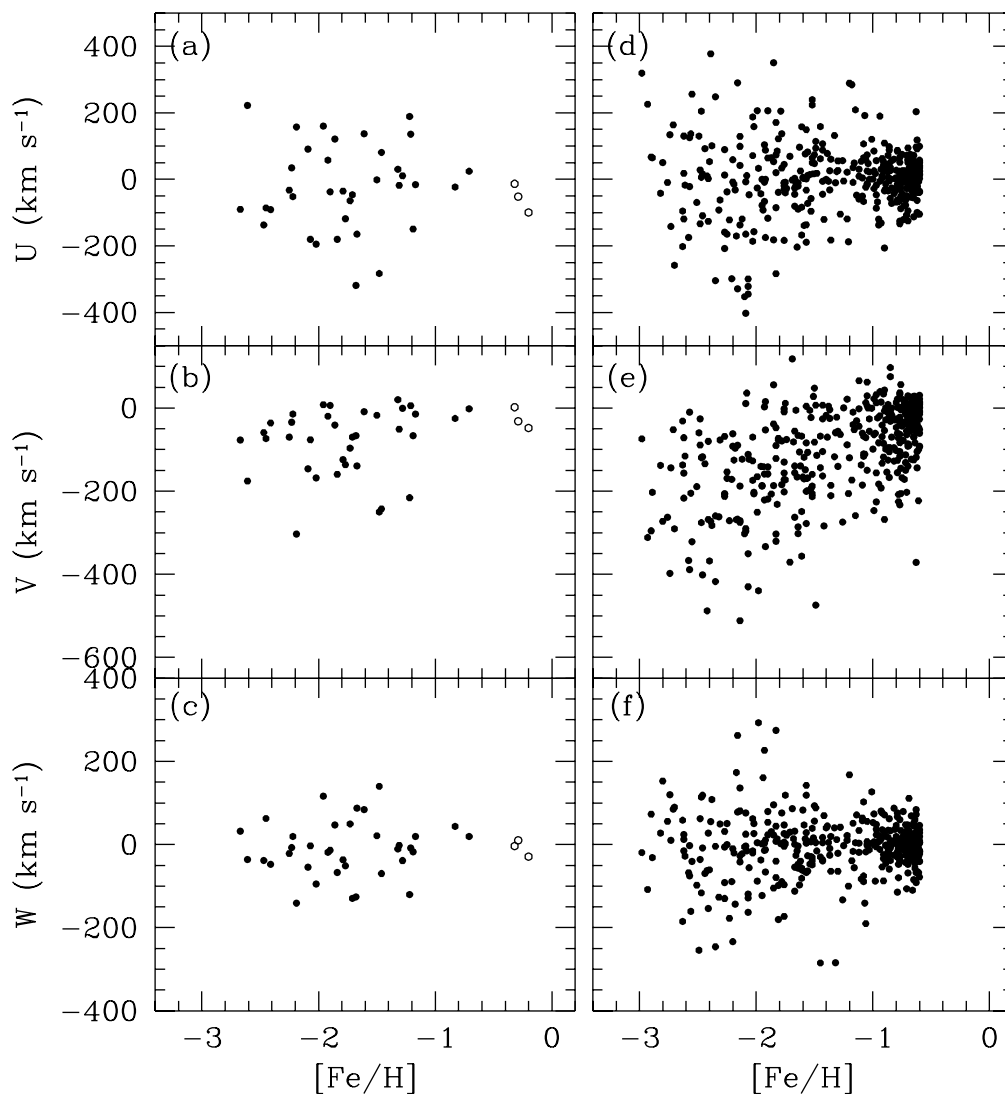
FIG. 2.—Local velocity components, U, V, and W, for (a–c) the LSE giants and (d–f) a sample of bright giants with $V \leq 12$ and [Fe/H] ≤ -0.6 from the Beers et al. (2000) catalog. The three points depicted with open circles in (a–c) are classified as either TO or FHB.

two-sample K-S test supports these impressions. The hypothesis that the two samples are drawn from a common parent is rejected with probability $p = 0.042$ (two-sided). A one-sided test, where the alternative hypothesis is that the LSE stars are drawn from a population of higher mean rotation, is, of course, an even stronger rejection.

Figures 3c and 3d show similar plots as described above, but for the metallicity cut [Fe/H] ≤ -1.6, the metallicity below which most previous authors have argued that the MWTD ceases to make an important contribution to the local volume density of metal-poor stars. Note that while the distribution of the 100 stars in the comparison sample

TABLE 9
MEAN VELOCITIES AND VELOCITY DISPERSIONS OF THE SAMPLE

[Fe/H] (dex)	N	$\langle U \rangle$ (km s^{-1})	$\langle V \rangle$ (km s^{-1})	$\langle W \rangle$ (km s^{-1})	σ_U (km s^{-1})	σ_V (km s^{-1})	σ_W (km s^{-1})
LSE Stars:							
≤ -0.6	36	-24 ± 22	-82 ± 14	-11 ± 11	130 ± 15	81 ± 10	66 ± 8
-0.6 to -1.6	12	-2 ± 35	-72 ± 29	-2 ± 18	122 ± 26	102 ± 22	63 ± 13
≤ -1.6	24	-35 ± 27	-87 ± 14	-16 ± 14	134 ± 20	71 ± 10	69 ± 10
Comparison stars:							
≤ -0.6	412	1 ± 5	-98 ± 6	-4 ± 3	101 ± 4	115 ± 4	68 ± 2
-0.6 to -1.6	278	8 ± 4	-57 ± 5	-2 ± 3	69 ± 3	85 ± 4	50 ± 2
≤ -1.6	134	-12 ± 13	-183 ± 11	-9 ± 8	146 ± 9	122 ± 7	94 ± 6

LSE Giants ([Fe/H] < -1.0)

V_ϕ (km/s)

LSE Giants ([Fe/H] < -1.0)

V_ϕ (km/s)

Comparison Sample ([Fe/H] < -1.0)

V_ϕ (km/s)

Comparison Sample ([Fe/H] < -1.0, -60 < l < +60)

V_ϕ (km/s)

LSE Giants ([Fe/H] < -1.6)

V_ϕ (km/s)

LSE Giants ([Fe/H] < -1.6)

V_ϕ (km/s)

Comparison Sample ([Fe/H] < -1.6)

V_ϕ (km/s)

Comparison Sample ([Fe/H] < -1.6, -60 < l < +60)

V_ϕ (km/s)
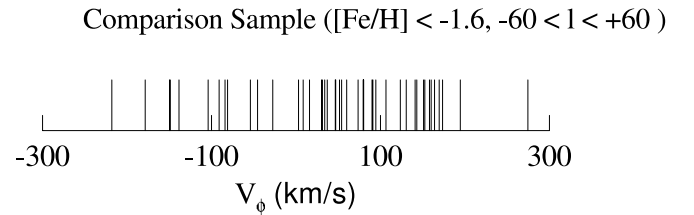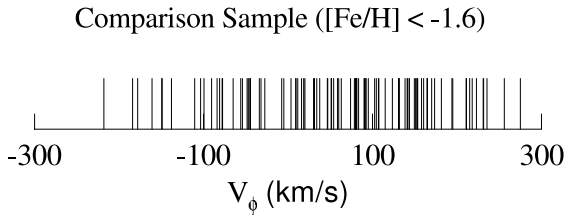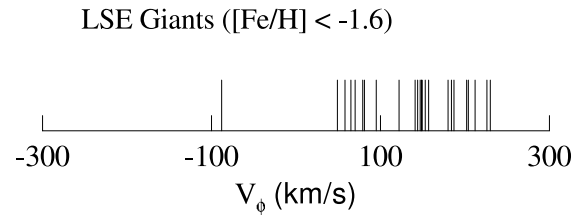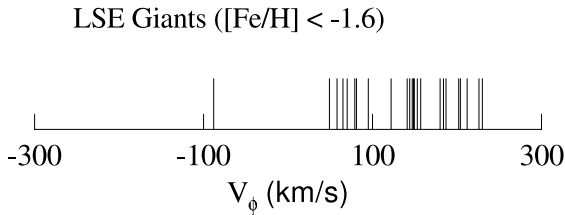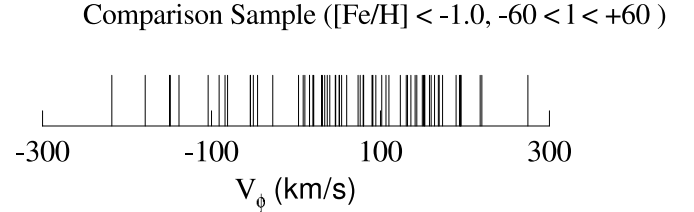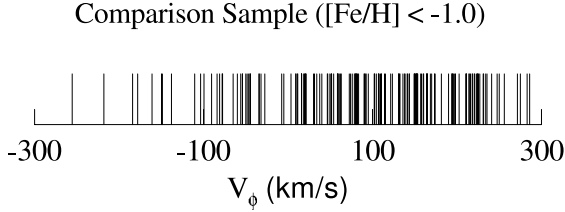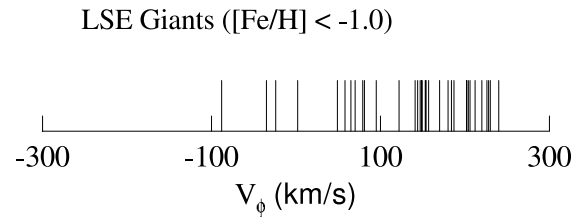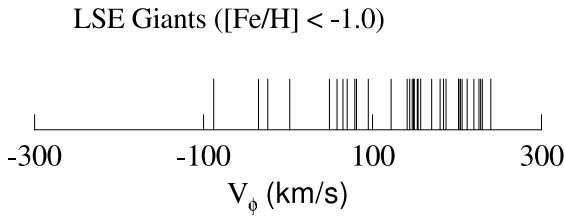
FIG. 3.—Stripe density plots of the derived rotational velocity component V_ϕ for LSE giants with $[Fe/H] \leq -1.0$, giants in the comparison sample with $[Fe/H] \leq -1.0$, LSE giants with $[Fe/H] \leq -1.6$, and giants in the comparison sample with $[Fe/H] \leq -1.6$. Note that the LSE giants exhibit a higher fraction of stars with large (positive) V_ϕ than the comparison sample for both metallicity cuts.

FIG. 4.—Same as Fig. 3, but for LSE giants with $[Fe/H] \leq -1.0$, giants in the comparison sample with $[Fe/H] \leq -1.0$ and selected in a longitude interval similar to the LSE giants, LSE giants with $[Fe/H] \leq -1.6$, and giants in the comparison sample with $[Fe/H] \leq -1.6$ and selected in a longitude interval similar to the LSE giants. The distributions still appear quite different from one another at both metallicity cuts.

seen in Figure 3d is broad and roughly symmetric about $V_\phi \approx 50$ km s^{-1}, consistent with its being composed primarily of halo objects, the distribution of the 24 LSE stars in Figure 3c is clearly centered on much higher rotational velocities; in fact, the lower cut on metallicity has removed most of the LSE stars we might have associated with the halo population! Not surprisingly, a K-S test rejects the likelihood of these samples sharing a common parent at a very high level, $p = 0.006$ (two-sided).

One might wonder whether some selection bias has produced the rather different distributions of V_ϕ described above. After all, the comparison sample was drawn from numerous samples covering much of the high Galactic latitude sky, while the LSE sample came from a more limited range in Galactic longitude ($-60° \leq l \leq +60°$) at lower lati-

tudes. In fact, the selection is rather stronger than this, since absorption toward the Galactic center has eliminated most of the sample within 30° of $l = 0°$, as can be seen from inspection of Table 1. To assess whether the different longitude selections have conspired to produce the rather different V_ϕ distributions, Figure 4 shows similar diagrams as in Figure 3, but with the LSE longitude cuts included in the subselection of the comparison sample. Although there are, of course, fewer stars in the comparison sample after these restrictions, the visual impression of the difference in the distributions remains. A two-sample K-S test of the subsamples of 34 LSE stars and 103 comparison-sample stars with $[Fe/H] \leq -1.0$, shown in Figures 4a and 4b, respectively, rejects the common parent hypothesis at a high level, $p = 0.002$ (two-sided). For the 24 LSE stars and 67 compar-

ison-sample stars with [Fe/H] ≤ -1.6 shown in Figures 4c and 4d, respectively, the rejection is even stronger, $p = 0.001$ (two-sided).

Figure 5a shows the relation between e and [Fe/H] for the LSE stars. There clearly exists a nonnegligible fraction of low-eccentricity metal-poor stars in this sample (again, the three nongiants are shown with open circles). Over 60% (22 of 36) of the LSE giants exhibit eccentricities less than $e = 0.5$. Figure 5b shows these same quantities for the comparison sample. In this panel, the filled circles represent the stars in the Galactic longitude range $-60° \leq l \leq +60°$, while the open circles represent the stars outside of this range. The visual impression one obtains is that the numbers of stars at low metallicity and low eccentricity in the comparison sample has been *decreased* by the application of the cuts in Galactic longitude that are pertinent to the LSE sample. This runs counter to the notion that the longitude selection of the LSE sample has somehow overemphasized the importance of the low-eccentricity stars. In fact, one

might be tempted to conclude that more complete longitude coverage at low latitudes would be likely to boost the relative numbers of low-metallicity, low-eccentricity stars.

For a more quantitative comparison, we show in Figure 6a the cumulative e distributions, $N(<e)$, in the abundance ranges [Fe/H] ≤ -1.0 (*thin dashed histogram*) and [Fe/H] ≤ -1.6 (*thin solid histogram*) for the 36 LSE giants, all of which have $|Z| < 1$ kpc. In this same panel, we also plot $N(<e)$ for the comparison sample of bright giants with $|Z| < 1$ kpc. Inspection of this figure suggests that the LSE sample contains more nearly circular orbits at [Fe/H] ≤ -1.6 than the comparison sample (*thick solid histogram*), whereas at [Fe/H] ≤ -1.0 (the thick dashed histogram representing the comparison sample) the difference, if any, in $N(<e)$ is less clear. An anonymous referee pointed out that it appeared from inspection of Figure 5 that the
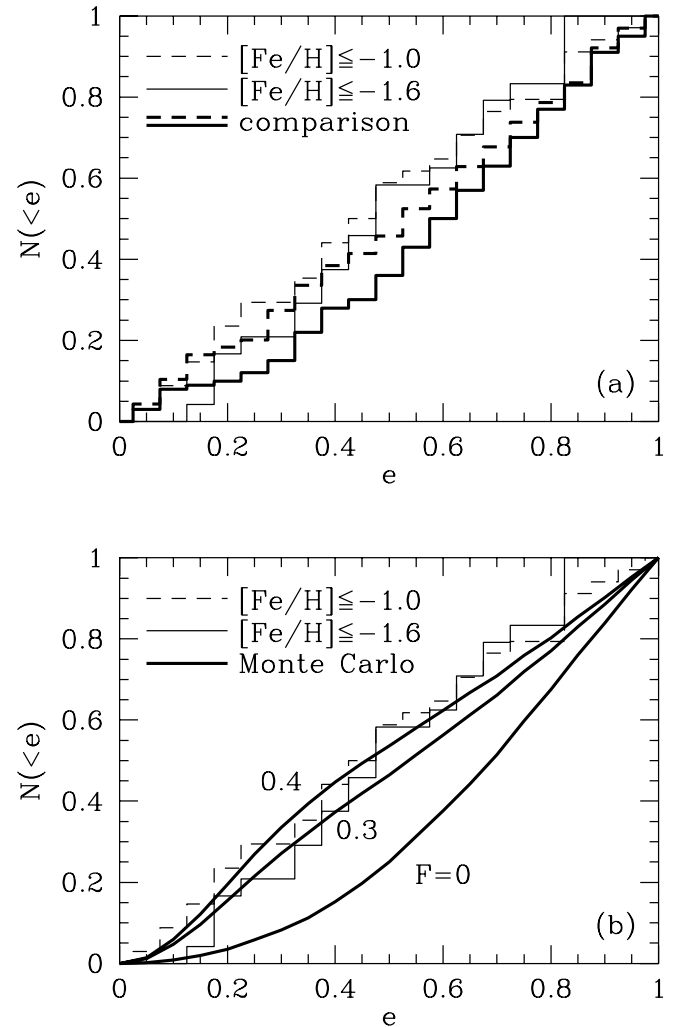

FIG. 5.—(a) Distribution of [Fe/H] for the LSE giants as a function of derived orbital eccentricity. Note the presence of substantial numbers of stars with quite low metallicity even for $e \leq 0.5$. Open circles indicate the nongiants. (b) The same as in (a), but for the giants in the comparison sample. In this panel, the filled circles represent stars chosen to satisfy $-60° \leq l \leq +60°$, while the open circles represent stars outside of this longitude range.

FIG. 6.—(a) Cumulative eccentricity distributions of the LSE giants for metallicity cuts of [Fe/H] ≤ -1.0 (*thin dashed histogram*) and [Fe/H] ≤ -1.6 (*thin solid histogram*). The thick dashed and solid histograms denote the comparison sample of giant stars at $|Z| < 1$ kpc in these same abundance ranges. (b) Comparison of the cumulative eccentricity distributions of the LSE giants with Monte Carlo models, based on a mixture of two Gaussian components taken to represent the halo and thick disk, where the disk fraction is denoted as F. We take $\langle V_\phi \rangle = 33$ km s^{-1} and $(\sigma_U, \sigma_V, \sigma_W) = (141, 106, 94)$ km s^{-1} for the halo and $\langle V_\phi \rangle = 200$ km s^{-1} and $(\sigma_U, \sigma_V, \sigma_W) = (46, 50, 35)$ km s^{-1} for the thick disk.

"halo objects," which one might loosely define to be those with eccentricities exceeding $e = 0.5$, appeared to have somewhat lower metallicities than expected if fair draws were made from the halo population. This effect, if real (small number statistics prevent any solid judgement to be made), is surely driven by the original selection of the LSE giants as metal-poor candidates. In any event, the same selection criteria were used for all of the candidate stars prior to any knowledge of their kinematics, hence the differential comparisons we have carried out are still meaningful.

A two-sample K-S test indicates that the eccentricity distributions for the cut in metallicity $[Fe/H] \leq -1.0$ cannot be distinguished; rejection of the hypothesis that the subsamples are drawn from the same parent population is not significant ($p = 0.25$, one-sided, vs. the alternative that the LSE stars are drawn from a parent population with lower eccentricity). However, for the cut in metallicity $[Fe/H] \leq -1.6$, a K-S test is able to reject the common parent population hypothesis at a marginally significant level, $p = 0.055$ (one-sided). The "near rejection" of the subsample of stars with $[Fe/H] = -1.6$ is certainly suggestive, although not yet definitive. Interestingly, when we apply the longitude cuts to the comparison subsample, as discussed above, in order to make it match the longitude distribution of the LSE subsample, it is possible to significantly reject the common parent hypothesis for both of the metallicity cuts; for $[Fe/H] \leq -1.0$, $p = 0.022$ (one-sided), and for $[Fe/H] \leq -1.6$, $p = 0.009$ (one-sided).

The above analysis certainly indicates a clearer signature of the MWTD population if the sample is selected at low Galactic latitude, as in the present work. To confirm this, we estimate the contribution of the thick disk component, F_{MWTD}, among local samples of metal-poor stars, using the derived distribution of e. Following the method developed by Chiba & Yoshii (1998), we have performed a Monte Carlo simulation to predict the e distribution from a mixture of stars contributed by the thick disk and halo populations. The characteristic kinematic parameters for these components are drawn from Chiba & Beers (2000): $\langle V_\phi \rangle = 33$ km s^{-1} and $(\sigma_U, \sigma_V, \sigma_W) = (141, 106, 94)$ km s^{-1} for the halo, and $\langle V_\phi \rangle = 200$ km s^{-1} and $(\sigma_U, \sigma_V, \sigma_W) = (46, 50, 35)$ km s^{-1} for the thick disk. Figure 4b (*thick solid line*) shows the results of this exercise for $F_{MWTD} = 0$, $F_{MWTD} = 0.3$, and $F_{MWTD} = 0.4$. It is evident that the eccentricity distribution of the LSE giants with $[Fe/H] \leq -1.6$ is characterized by $F_{MWTD} \sim 0.3$, substantially larger than the estimate of $F_{MWTD} \sim 0.1$ derived from the sample considered by Chiba & Beers (2000). With the metallicity cut $[Fe/H] \leq -1.0$, the value of $F_{MWTD} = 0.4$ appears to be a superior fit. *Both results strongly suggest that previous nonkinematic selection of metal-poor stars at higher Galactic latitudes has resulted in a severe underestimate of the relative importance of the MWTD in local samples.*

3.3. Assignment of Population Membership

As seen from the discussion above, many of the LSE stars exhibit rather small V velocities, suggesting that they may belong to a rapidly rotating (thick) disk component; we now attempt to assign the likely population membership of each LSE star based on its full space motion. This is clearly an inexact procedure, since the halo population exhibits large dispersions in all of its velocity components. If the motion of a star is well outside an acceptable range of the character-

istic spatial and velocity distributions of the thick disk, it is most likely a member of the halo population, otherwise it belongs to *either* the disk or halo population, and we cannot uniquely determine its membership.

The velocity distribution of the thick disk component was determined by Chiba & Beers (2000) using a large number of stars from the Beers et al. (2000) catalog, summarized as $\langle V_\phi \rangle_{disk} = 200$ km s^{-1} and $(\sigma_{U,disk}, \sigma_{V,disk}, \sigma_{W,disk}) = (46, 50, 35)$ km s^{-1}. We also adopt $|Z| \leq 1$ kpc as a typical vertical range of the thick disk (Chiba & Yoshii 1998; Chiba & Beers 2000). If a star exhibits $|Z_{max}| > 1$ kpc or at least one of its velocity components deviates from the above velocity range of the disk at more than a 2σ level, we assign it to the halo population, denoted as "H" in column (14) of Table 8. On the other hand, a star within the above range of the disk at less than a 2σ level might belong to either the disk or halo population, which we label as "DH" in column (14). The three stars with metallicities $[Fe/H] > -0.50$ also exhibit space motions expected for membership in a disk population, hence we assign the classification "D" in column (14).

Since there is great interest in searches for any chemical signature of the origin of the MWTD, we have noted with footnotes the stars in Table 8 that are classified as "DH," but having low (absolute values of) individual velocity components (taken here to mean $|U, V, W| \leq 50$ km s^{-1}), and that further satisfy the requirements $V_\phi \geq 170$ km s^{-1}, $Z_{max} < 1$ kpc, and $[Fe/H] = -0.6$, suggesting that they may indeed be bona fide members of the MWTD, and hence deserving of detailed study at high resolution. This sample may not be pure, but it seems likely that at least a number of these stars are members of the MWTD population. Note that the familiar metal-poor giant HD 184711 (=LSE 149) just misses designation as a likely member of the MWTD, since its V velocity component is somewhat higher than the above criteria allow.

4. SUMMARY AND DISCUSSION

We have presented spectroscopy and photometry for a small sample of bright metal-deficient giant candidates selected from a prism survey (the LSE survey of Drilling & Bergeron 1995) that explores lower Galactic latitudes than most previous surveys for metal-deficient stars. Estimates of metallicity for the stars in this sample have been obtained by a variety of methods, all in good agreement with one another. Since all of our program stars have available proper motions, we were able to derive estimates of their complete space motions and orbital eccentricities.

Inspection of the distribution of rotational velocities for the LSE stars indicates that they cannot be drawn from the same parent population as stars from previous samples of similarly bright giants (generally selected at higher Galactic latitude), such as described by Beers et al. (2000); many individual stars appear to be rotating quite rapidly about the Galactic center. Furthermore, inspection of the distribution of orbital eccentricity for the LSE giants, as contrasted with that of the same comparison sample of bright giants, has revealed that the LSE sample contains a much larger proportion of metal-weak stars with low eccentricities, as might be expected if the MWTD population is an important component in the solar neighborhood. Our best estimates of the fraction of local MWTD stars, based on Monte Carlo models of the expected distribution of orbital eccentricities of a pure halo population, suggest $F_{MWTD} \approx 40\%$ for the

metallicity regime $[Fe/H] \leq -1.0$ and remain as high as $F_{MWTD} \approx 30\%$ for the metallicity regime $[Fe/H] \leq -1.6$. This fraction is *triple* the value obtained for stars with $[Fe/H] \leq -1.6$ in the Chiba & Beers (2000) analysis of the stars in the Beers et al. (2000) catalog. The lowest metallicity star in the LSE sample with kinematics that are consistent with membership of the MWTD population is LSE 156, with $[Fe/H] = -2.35$.

Over the past decade, a number of claims for a significant population of metal-poor stars with disklike kinematics have been made, but acceptance of their presence has been cast in doubt because of incorrectly assigned metallicities. Based on this new sample, this no longer appears to be the case, and we must endeavor to understand the implications of a significant population of MWTD stars for theories of the formation and evolution of the Galaxy. In this respect, it is important to keep in mind that, although the MWTD population may contribute a large fraction of the *local* metal-poor stars, the (inner) halo population is probably still the dominant reservoir of stars with $[Fe/H] \leq -1.6$ within a few kiloparsecs of the Sun. Furthermore, although we have emphasized the possible importance of the MWTD population, it certainly appears to be a minor constituent of the entire thick disk population; Martin & Morrison (1998) suggest that the local density of the MWTD represents less than 1% of that of the canonical thick disk.

It is of interest to note that the comparison of $[Fe/H]$ versus orbital eccentricity diagrams of Chiba & Beers (2000) with the numerical models of hierarchical galaxy formation of Bekki & Chiba (2001) suggested that the models were *overproducing* the expected numbers of metal-poor stars with low eccentricities relative to the observations (see Fig. 14 of Bekki & Chiba 2001), at least in the intermediate abundance range $-1.6 \leq [Fe/H] \leq -1.0$. It now seems likely that the problem may lie, at least in part, with the observations themselves, which have not extended to sufficiently low Galactic latitudes to fairly sample the presence of MWTD stars.

If, as we have argued, there does indeed exist a significant fraction of thick disk stars with metal abundances $[Fe/H] \leq -1.6$, this finding may have significance to formation scenarios for the Milky Way and, by inference, for other large spiral galaxies. One currently plausible explanation for the origin of a MWTD component may be the merging of small proto-Galactic fragments (e.g., Searle & Zinn 1978) with a preexisting thin, possibly metal-poor, stellar disk (e.g., Quinn, Hernquist, & Fullagar 1993; Wyse 2001). Such fragments may correspond to the progenitors of the present-day luminous dwarf satellites, such as Sagittarius (Ibata, Gilmore, & Irwin 1994), or some of the numerous cold dark matter subhalos surrounding the Galaxy, as predicted from recent cosmological simulations (e.g., Klypin et al. 1999; Moore et al. 1999). Minor merging events might also explain the origin of the rapidly rotating, thick disk globular clusters (Bekki & Chiba 2002). Recent identification of various streamlike features in the halo (and possibly near the disk) may be associated with the debris of these past merging events (Wyse et al. 2000; Newberg et al. 2002). Dinescu (2002) has argued, from a close inspection of the Beers et al. (2000) sample, for the presence of a retrograde population that exhibits similarities to the orbit of the globular cluster ω Centauri. Derivation of a more precise estimate of the fractional contribution of the MWTD component in the solar neighborhood will help set limits on the merging process(es) in the early (and possibly more recent) Galaxy.

One key piece of information for the likely source of the MWTD stars is obtainable by study of the relative abundance patterns of individual elements for stars of the thick disk population. Recently, Prochaska et al. (2000) have carried out such a study based on 10 stars with disklike kinematics chosen from the proper-motion–selected survey of Carney et al. (1994), covering the metallicity range $-1.0 \leq [Fe/H] \leq -0.4$, the range most pertinent to the canonical thick disk. These authors concluded that the thick disk elemental abundance patterns were essentially identical to those for stars of the halo population, consistent with the idea that the two populations share similar nucleosynthesis histories. It is of obvious importance to extend such studies to lower metallicities, such as could be accomplished by abundance analyses of the LSE stars noted in the present paper, to see if this result applies to stars in the abundance range $-2.5 \leq [Fe/H] \leq -1.0$. Another useful set of targets for high-resolution studies may be found in Table 6 of Chiba & Beers (2000). This last point is crucial, since previous studies of Galactic chemical evolution have generally adopted the view that stars with metallicities below $[Fe/H] \approx -1$ represent an essentially pure halo population. Unless caution is taken (for example, by only using those stars with inferred distances more than a few kiloparsecs above the disk plane or with kinematics that are indisputably associated with the halo), there is the clear danger of confounding the sample with mixed populations.

Clearly, it would also be important to carry out further surveys for the detection of bright (hence nearby) metal-poor stars at lower Galactic latitudes. One attractive sample could be assembled from the extensive reclassifications of the HD catalog stars by Houk et al. (Houk & Swift 1999, and references therein). Inspection of the available data reveals that there are several hundred bright F- and G-type stars, classified as possibly metal-deficient, located at Galactic latitudes $|b| \leq 30°$, many of which already have available proper motions. A medium-resolution spectroscopic survey of these stars is just now getting underway and should provide important constraints on the MWTD population in the near future.

REFERENCES

Arce, H. G., & Goodman, A. A. 1999, ApJ, 512, L135
Beers, T. C., Chiba, M., Yoshii, Y., Platais, I., Hanson, R. B., Fuchs, B., & Rossi, S. 2000, AJ, 119, 2866
Beers, T. C., Rossi, S., Norris, J. E., Ryan, S. G., & Shefler, T. 1999, AJ, 117, 981
Beers, T. C., & Sommer-Larsen, J. 1995, ApJS, 96, 175
Bekki, K., & Chiba, M. 2001, ApJ, 558, 666
———. 2002, ApJ, 566, 245
Bond, H. E. 1980, ApJS, 44, 517
Bonifacio, P., Centurion, M., & Molaro, P. 1999, MNRAS, 309, 533
Burris, D. L., Pilachowski, C. A., Armandroff, T. E., Sneden, C., Cowan, J. J., & Roe, H. 2000, ApJ, 544, 302
Burstein, D., & Heiles, C. 1982, AJ, 87, 1165
Carney, B. W., Latham, D. W., Laird, J. B., & Aguilar, A. 1994, AJ, 107, 2240
Chiba, M., & Beers, T. C. 2000, AJ, 119, 2843
Chiba, M., & Yoshii, Y. 1998, AJ, 115, 168
Chiba, M., Yoshii, Y., & Beers, T. C. 1999, in ASP Conf. Ser. 165, The Third Stromlo Symposium: The Galactic Halo, ed. B. K. Gibson, T. S. Axelrod, & M. E. Putman (San Francisco: ASP), 273
Dinescu, D. I. 2002, in ASP Conf. Ser. 265, Omega Centauri: A Unique Window into Astrophysics, ed. F. van Leeuwen, G. Piotto, & J. Hughes (San Francisco: ASP), in press
Drilling, J. S., & Bergeron, L. E. 1995, PASP, 107, 846
ESA. 1997, The Hipparcos and Tycho Catalogues (ESA SP-1200) (Noordwijk: ESA)
Fuhrmann, K. 1998, A&A, 338, 161
Høg, E., et al. 2000, A&A, 355, L27
Houk, N., & Swift, C. 1999, Michigan Catalog of Two-dimensional Spectral Types for the HD Stars, Vol. 5 (Ann Arbor: Univ. Michigan)
Ibata, R., Gilmore, G. F., & Irwin, M. J. 1994, Nature, 370, 194
Johnson, H. L. 1963, in Basic Astronomical Data, ed. K. A. Strand (Chicago: Univ. Chicago Press), 204
Johnson, H. L., Mitchell, R. I., Iriarte, B., & Wisniewski, W. Z. 1966, Comm. Lunar Plan. Lab., 4, 99
Katz, D., et al. 1999, Ap&SS, 265, 221
Klypin, A., Kravtsov, A. V., Valenzuela, O., & Prada, F. 1999, ApJ, 522, 82
Landolt, A. U. 1973, AJ, 78, 959
Layden, A. 1995, AJ, 110, 2288

Martin, J. C., & Morrison, H. L. 1998, AJ, 116, 1724
Mashonkina, L., & Gehren, T. 2000, A&A, 364, 249
McWilliam, A., Preston, G. W., Sneden, C., & Searle, L. 1995a, AJ, 109, 2757
McWilliam, A., Preston, G. W., Sneden, C., & Shectman, S. 1995b, AJ, 109, 2736
Mihalas, D., & Binney, J. 1981, Galactic Astronomy: Structure & Kinematics (2d ed.; San Francisco: Freeman)
Moore, B., Ghigna, S., Governato, F., Lake, G., Quinn, T., & Stadel, J. 1999, ApJ, 524, L19
Morrison, H. L. 1993, AJ, 105, 539
Morrison, H. L., Flynn, C., & Freeman, K. C. 1990, AJ, 100, 1191
Morrison, J. E., Röser, S., Lasker, B. M., Smart, R. L., & Taff, L. G. 1996, AJ, 111, 1405
Newberg, H. J., et al. 2002, ApJ, 569, 245
Norris, J., Bessell, M. S., & Pickles, A. J. 1985, ApJS, 58, 463
Norris, J. E., Ryan, S. G., & Beers, T. C. 2001, ApJ, 561, 1034
Prochaska, J. X., Naumov, S. O., Carney, B. W., McWilliam, A., & Wolfe, A. M. 2000, AJ, 120, 2513
Quinn, P. J., Hernquist, L., & Fullagar, D. P. 1993, ApJ, 403, 74
Ryan, S. G., & Lambert, D. 1995, AJ, 109, 2068
Ryan, S. G., & Norris, J. E. 1991, AJ, 101, 1835
Schlegel, D. J., Finkbeiner, D. P., & Davis, M. 1998, ApJ, 500, 525
Schulte, D. H., & Crawford, D. L. 1961, Kitt Peak Nat. Obs. Contrib., No. 10
Searle, L., & Zinn, R. 1978, ApJ, 225, 357
Skrutskie, M. F., et al. 1997, in The Impact of Large Scale Near-IR Sky Surveys, ed. F. Garzon et al. (Dordrecht: Kluwer), 187
Snider, S., Allende-Prieto, C., von Hippel, T., Beers, T. C., Sneden, C., Qu, Y., & Rossi, S. 2001, ApJ, 562, 528
Sommer-Larsen, J., & Zhen, C. 1990, MNRAS, 242, 10
Spite, M., Spite, F., Cayrel, R., Hill, V., Nördstrom, B., Barbuy, B., Beers. T. C., & Nissen, P. E. 1999, Ap&SS, 265, 141
Stephenson, C. B., & Sanduleak, N. 1971, Publ. Warner Swasey Obs., 1, 1
Twarog, B. A., & Anthony-Twarog, B. J. 1994, AJ, 107, 1371
Wyse, R. F. G. 2001, in ASP Conf. Ser. 230, Galaxy Disks and Disk Galaxies, ed. J. G. Funes & E. M. Corsini (San Francisco: ASP), 71
Wyse, R. F. G., Gilmore, G., Norris, J. E., & Freeman, K. C. 2000, BAAS, 197, 41.15